Article

Cancer Cell

Age-Related Gliosis Promotes Central Nervous System Lymphoma through CCL19-Mediated Tumor Cell Retention

Graphical Abstract

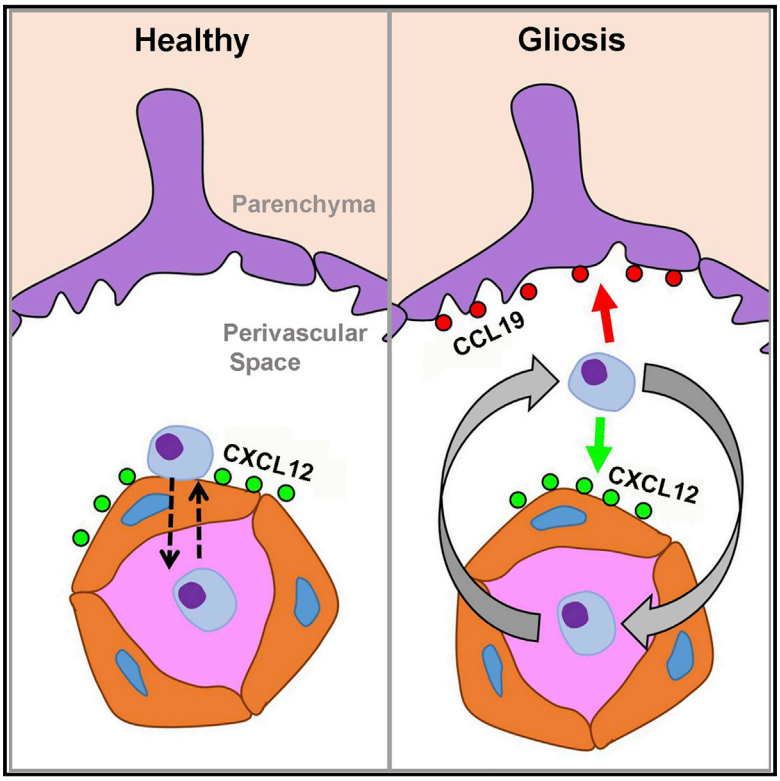

Highlights

- Gliosis increases the risk for central nervous system lymphoma
- Lymphoma cell enter the healthy brain parenchyma but exit quickly due to endothelial CXCL12
- Astrocytic CCL19 counteracts CXCL12 and retains lymphoma cells in the parenchyma
- Aged brains express more CCL19 and are more susceptible to forming CNS lymphomas

Authors

Tracy O'Connor, Xiaolan Zhou, Jan Kosla, ..., Louisa von Baumgarten, Ulrich Keller, Mathias Heikenwalder

Correspondence

tracy.oconnor@helmholtz-muenchen.de (T.O.), m.heikenwaelder@dkfz-heidelberg.de (M.H.)

In Brief

O'Connor et al. show that lymphoma cells (LCs) enter the brain but quickly exit along an endothelial CXCL12 gradient, which is countered by astrocyte-derived CCL19. Aged and gliotic brains express more CCL19 and thus retain LCs longer, conferring an increased risk of developing central nervous system lymphoma.

O'Connor et al., 2019, Cancer Cell *36*, 250–267
September 16, 2019
https://doi.org/10.1016/j.ccell.2019.08.001

CellPress

CellPress

Cancer Cell
Article

Age-Related Gliosis Promotes Central Nervous System Lymphoma through CCL19-Mediated Tumor Cell Retention

Tracy O'Connor,[1,2,3,4,*] Xiaolan Zhou,[5,6] Jan Kosla,[1,2,4] Arlind Adili,[1,2] Maria Garcia Beccaria,[4] Elena Kotsiliti,[1,2,4] Dominik Pfister,[1,2,4] Anna-Lena Johlke,[1,2] Ankit Sinha,[7] Roman Sankowski,[8] Markus Schick,[9] Richard Lewis,[9] Nikolaos Dokalis,[8] Bastian Seubert,[1,2] Bastian Höchst,[3] Donato Inverso,[10] Danijela Heide,[4] Wenlong Zhang,[5] Petra Weihrich,[11] Katrin Manske,[3] Dirk Wohlleber,[3] Martina Anton,[3] Alexander Hoellein,[9]

(Author list continued on next page)

[1]Institute of Virology, Technical University of Munich, 81675 Munich, Germany
[2]Helmholtz Center Munich, 85764 Neuherberg, Germany
[3]Institute of Molecular Immunology and Experimental Oncology, Technical University of Munich, Ismaningerstraße 22, 81675 Munich, Germany
[4]Division of Chronic Inflammation and Cancer, German Cancer Research Center (DKFZ), Im Neuenheimer Feld 242, 69120 Heidelberg, Germany
[5]Department of Neurology, Ludwig-Maximilians-University Hospital Munich, 81377 Munich, Germany
[6]Department of Rehabilitation, Shengjing Hospital of China Medical University, Shenyang, Liaoning, China
[7]Experimental Systems Immunology, Max Planck Institute of Biochemistry, Munich, Germany
[8]Institute of Neuropathology, Medical Faculty, University of Freiburg, 79085 Freiburg, Germany
[9]III. Medical Department, Technical University of Munich, 81675 Munich, Germany
[10]Division of Vascular Oncology and Metastasis, German Cancer Research Center Heidelberg (DKFZ-ZMBH Alliance), 69120 Heidelberg, Germany

(Affiliations continued on next page)

SUMMARY

How lymphoma cells (LCs) invade the brain during the development of central nervous system lymphoma (CNSL) is unclear. We found that NF-κB-induced gliosis promotes CNSL in immunocompetent mice. Gliosis elevated cell-adhesion molecules, which increased LCs in the brain but was insufficient to induce CNSL. Astrocyte-derived CCL19 was required for gliosis-induced CNSL. Deleting CCL19 in mice or CCR7 from LCs abrogated CNSL development. Two-photon microscopy revealed LCs transiently entering normal brain parenchyma. Astrocytic CCL19 enhanced parenchymal CNS retention of LCs, thereby promoting CNSL formation. Aged, gliotic wild-type mice were more susceptible to forming CNSL than young wild-type mice, and astrocytic CCL19 was observed in both human gliosis and CNSL. Therefore, CCL19-CCR7 interactions may underlie an increased age-related risk for CNSL.

INTRODUCTION

The 1-year overall survival rate of peripheral diffuse large B cell lymphoma (DLBCL) is ~85% (Horvat et al., 2018). However, prognosis of patients with primary central nervous system lymphoma (PCNSL) is markedly poorer, with a one-year overall survival rate of 50%–60% (Ferreri et al., 2016; Fritsch et al., 2017). Lymphomas also disseminate to the central nervous system

Significance

The central nervous system (CNS) is excluded from routine surveillance by the adaptive immune system. Nevertheless, malignancies derived from adaptive immune cells, such as lymphomas, occur in the CNS. Unexpectedly, using *in vivo* imaging, we found that lymphoma cells (LCs) frequently entered the normal CNS, although formation of mature CNSL from single LCs was rare. The vast majority of LCs left the CNS along an endothelial CXCL12 gradient. Gliosis in the brain and production of CCL19 by astrocytes counteracted CXCL12, enhanced LC retention, and increased the probability of CNSL formation. We identified gliosis, a pervasive condition associated with aging, as a risk factor for CNSL. Moreover, CCL19/CCR7-mediated LC retention might be exploited prophylactically to prevent LC dissemination to the CNS.

Gitta Seleznik,[12] Juliane Bremer,[12] Sabine Bleul,[13] Hellmut G. Augustin,[10,14,15] Florian Scherer,[13] Uwe Koedel,[5] Achim Weber,[16] Ulrike Protzer,[1,2] Reinhold Förster,[17] Thomas Wirth,[11] Adriano Aguzzi,[12] Felix Meissner,[7] Marco Prinz,[8,18,19] Bernd Baumann,[11] Uta E. Höpken,[20] Percy A. Knolle,[3] Louisa von Baumgarten,[5] Ulrich Keller,[9,15,21] and Mathias Heikenwalder[1,2,3,4,22,*]

[11]Institute for Physiological Chemistry, University of Ulm, 89081 Ulm, Germany
[12]Institute of Neuropathology, University Hospital of Zurich, 8091 Zurich, Switzerland
[13]Department of Hematology, Oncology and Stem Cell Transplantation, Freiburg University Medical Center, Albert-Ludwigs University, 79106 Freiburg, Germany
[14]European Center for Angioscience (ECAS), Medical Faculty Mannheim, Heidelberg University, Heidelberg, Germany
[15]German Cancer Consortium (DKTK), 69120 Heidelberg, Germany
[16]Department of Pathology and Molecular Pathology, University Hospital of Zurich, 8091 Zurich, Switzerland
[17]Institute of Immunology, Hannover Medical School, 30625 Hannover, Germany
[18]Signalling Research Centres BIOSS and CIBSS, University of Freiburg, Freiburg, Germany
[19]Center for Basics in NeuroModulation (NeuroModulBasics), Faculty of Medicine, University of Freiburg, Freiburg, Germany
[20]Max Delbrück Center for Molecular Medicine, 13092 Berlin, Germany
[21]Hematology and Oncology, Charité – Universitätsmedizin Campus Benjamin Franklin, 12200 Berlin, Germany
[22]Lead Contact
*Correspondence: tracy.oconnor@helmholtz-muenchen.de (T.O.), m.heikenwaelder@dkfz-heidelberg.de (M.H.)
https://doi.org/10.1016/j.ccell.2019.08.001

(CNS) from peripheral sites at a rate of 4%–5% ("secondary" CNSL [SCNSL]), and the prognosis for SCNSL is typically even poorer (Nagle et al., 2017). Since the advent of anti-retroviral therapy, HIV-associated CNSL has become less common (Villano et al., 2011). Hence, the majority of CNSLs currently occur in immunocompetent individuals (Alessandro et al., 2017; Sierra del Rio et al., 2009), and it is unclear how or why malignant cells of lymphoid origin invade the nervous tissue. Chronic inflammatory conditions elevate the risk for developing peripheral lymphomas (Smedby et al., 2006a, 2006b). A similar epidemiological link between neuroinflammation and a heightened risk for CNSL has not been reported; however, several components of the nuclear factor κB (NF-κB) signaling pathway (e.g., MYD88, the BCR pathway, and BAFF), are activated in CNSL lesions (Birnbaum et al., 2013; Deckert et al., 2014b; Krumbholz et al., 2005; Lee et al., 2017; Montesinos-Rongen et al., 2011). Moreover, a number of case studies indicate that demyelinating inflammatory disorders may precede CNSL development (Alderson et al., 1996; Hochberg et al., 2007; Husseini et al., 2012; Lu et al., 2016; Lyons et al., 2011). CXCL13, which is produced via NF-κB signaling, is strongly implicated in multiple sclerosis (MS) (Housley et al., 2015) and is highly expressed in CNSL (Fischer et al., 2009; Rubenstein et al., 2013; Tun et al., 2008). In secondary lymphoid organs, CXCL13, as well as other homeostatic chemokines, are produced downstream of the master cytokines lymphotoxin α (LTα) and LTβ. LTα and LTβ are also ectopically expressed in tertiary lymphoid organs (TLOs) during chronic inflammatory conditions (Ruddle, 2014). Thus, LTα and LTβ play a central role in orchestrating events during chronic inflammation. Based on this evidence, we hypothesized that chronic inflammation in the CNS may be a predisposing factor in the development of CNSL.

RESULTS

CNS Lymphotoxin Expression Induces Chronic Gliosis without Synaptic Loss or Blood-Brain Barrier Breakdown

To chronically activate alternative NF-κB in the CNS, we created transgenic mice expressing LTα and LTβ under the glial fibrillary acidic protein (GFAP) gene promoter. Three founder lines were obtained with low (#8) and high (#23 and #26) CNS expression of LTα and LTβ (Figures 1A and 1B). Line #26 was selected for further studies. Widespread astrogliosis and sporadic microgliosis were observed in the brain of 2-month-old GFAP-LTαβ mice by GFAP immunoblot (Figures S1A and S1B) and by GFAP and F4/80 immunohistochemistry (IHC) (Figures 1C and 1D). Increased *Iba1* expression indicated the presence of activated myeloid cells (Figure 1E). Enhanced major histocompatibility complex II (MHCII) immunoreactivity was observed in the brain parenchyma (Figures 1C and 1D) and choroid plexus (Figure S1C), as well as elevated MHCII transcript *H2-Aa* (Figure 1E). MHCII-expressing cells were $CD11b^+$ and $GFAP^-$ (Figures 1F and S1D). $CD11c^+$ cells were rare (Figure S1E). $CD4^+$ T cells were observed via IHC (Figures 1C and 1D), as well as increased *Cd3g* and *Il22* mRNA (Figures 1E and S1F), indicating enhanced T cell influx in GFAP-LTαβ brains. However, no B cells were observed in GFAP-LTαβ brains via IHC for B220 (Figure S1G) or mRNA analysis of *Cd19* (Figure S1H). No difference in PSD-95 immunoreactivity (Figure S1I) nor any significant decrease in PSD-95 (*Dlg4*) or synaptophysin mRNA was detected (Figure S1J), indicating no appreciable synaptic loss. Analysis of blood-brain barrier (BBB) integrity indicated that tight junctions were intact (Figures S1K–S1M). Expression of a number of additional pro-inflammatory molecules were significantly upregulated in GFAP-LTαβ brains including *Il6*, *Cxcl1*, *Ccl2*, *Tlr2*, *Ccl7*, and *Cxcl10*, and interleukin-33 (IL-33), whereas expression of *Cd200r* (on $CD45^+$ cells; Figure S1N) and myeloid homeostasis gene *Trem2* (Figures 1E and S1O) was downregulated. In addition, we performed a mass spectrometry-based proteomic comparison of GFAP-LTαβ and non-transgenic (NTg) brains, and identified a number of upregulated inflammatory pathways (Figures S1P–S1S). Taken together, these data indicate a mild shift from an anti- to a pro-inflammatory state in GFAP-LTαβ brains in the absence of any severe neuronal damage or BBB breakdown.

B Cell Lymphomas Preferentially Form in Nervous Tissue with Chronic Gliosis

To determine whether B cell lymphomas would form in GFAP-LTαβ CNS at a higher rate than NTg littermates, we injected

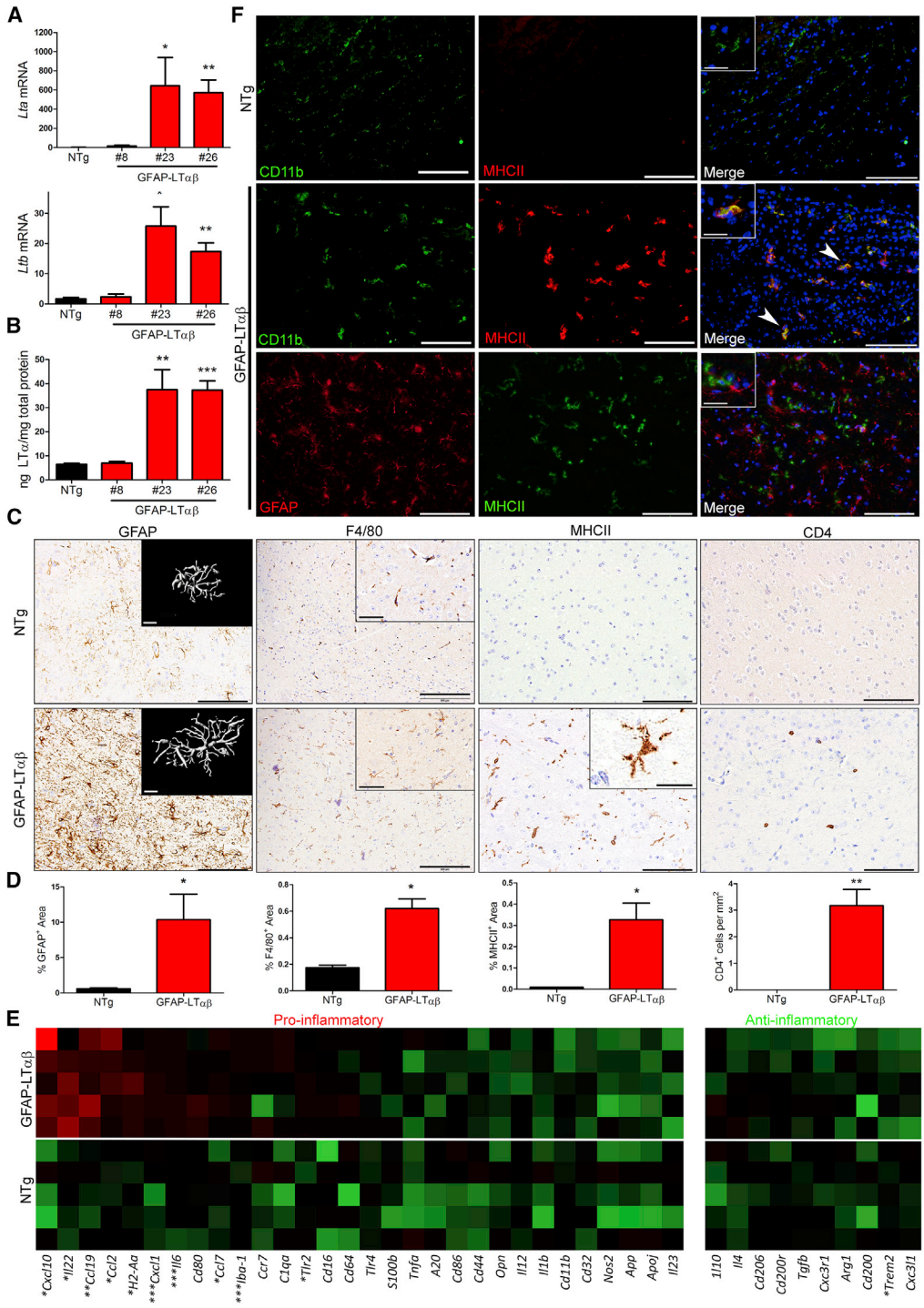

Figure 1. GFAP-LTαβ Mice Display Chronic Gliosis

(A and B) Total mRNA (A) or protein (B) was isolated from the brains of non-transgenic (NTg) or GFAP-LTαβ founder lines #8, #23, or #26 and analyzed for *Lta* or *Ltb* expression via qPCR (A) or LTα sandwich ELISA (B).

(C) Brain sections from GFAP-LTαβ#26 or NTg mice were stained for GFAP, F4/80, MHCII, or CD4. Scale bars, 100 μm; GFAP inset shows a 3D reconstruction of typical astrocytes in each genotype. Scale bar, 10 μm (F4/80 insets, 50 μm; MHCII inset, 25 μm).

(D) Quantifications of IHC stains in (C).

(E) mRNA from NTg or GFAP-LTαβ brains was used for qPCR analysis of the indicated genes.

(F) CoIF of MHCII with CD11b or GFAP in NTg and GFAP-LTαβ brains. White arrows, co-localization. Blue, DAPI. Scale bars, 100 μm (insets, 25 μm). n = 5–7 mice per group for each analysis.

All error bars denote SEM. See also Figure S1. *p < 0.05, **p < 0.01, ***p < 0.001.

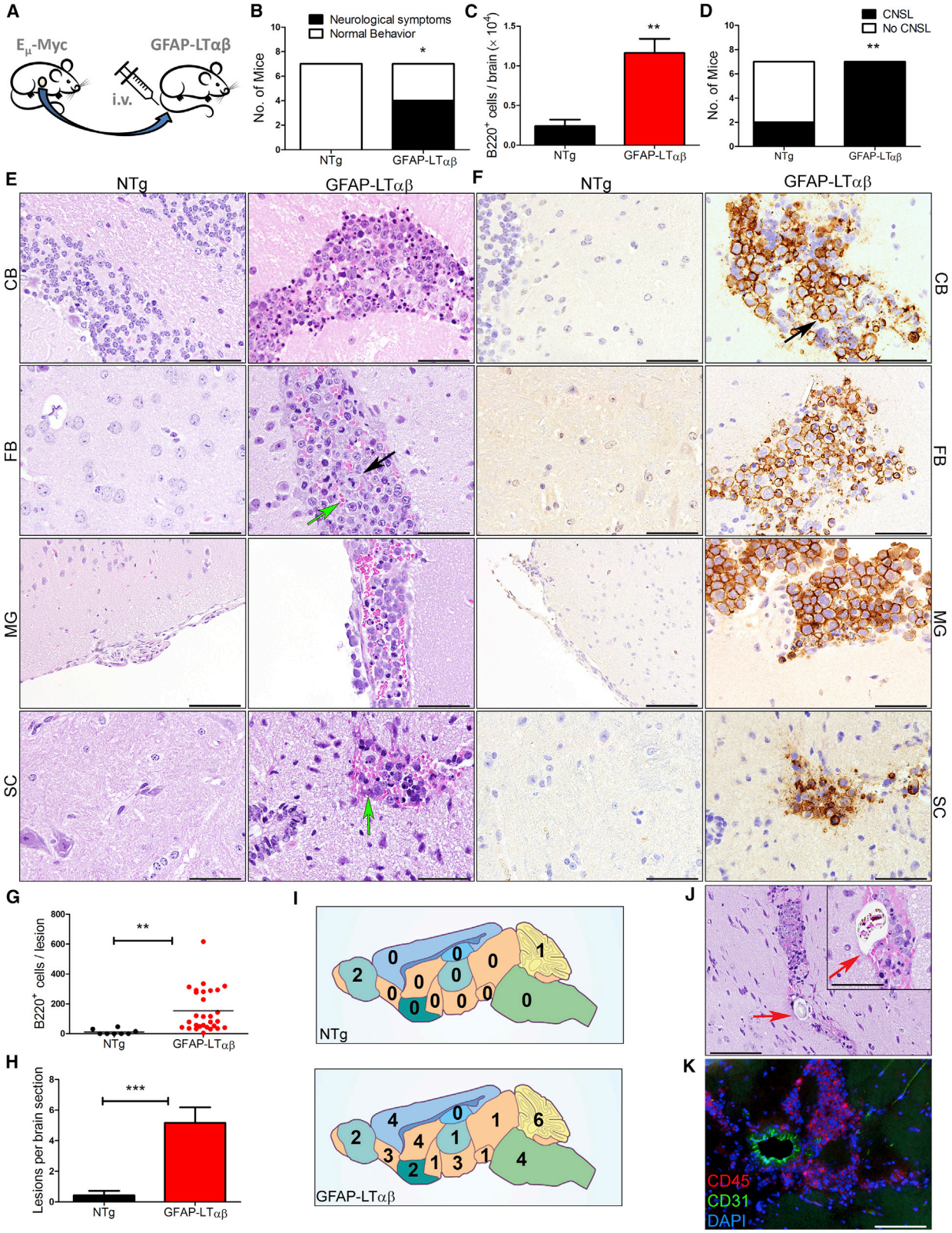

Figure 2. Chronic Gliosis Promotes the Formation of E_μ-Myc Lymphomas in the CNS

(A) GFAP-LTαβ and NTg mice were injected i.v. with an LC cell line derived from E_μ-Myc lymph nodes and analyzed at terminal disease.

(B) Incidence of neurological symptoms (ataxia/hindlimb paralysis) in GFAP-LTαβ mice versus NTg mice injected with LCs.

(legend continued on next page)

mice intravenously (i.v.) with a B cell LC line derived from lymphoid organs of mice expressing the Myc oncogene under the control of the B cell-specific immunoglobulin H locus enhancer, E_μ ("E_μ-Myc" mice) (Adams et al., 1985) (Figure 2A). Four weeks after injection, NTg and GFAP-LTαβ mice progressed to terminal illness at similar rates. Fifty-seven percent of GFAP-LTαβ mice developed neurological disturbances, which were absent in NTg mice (Figure 2B). Flow cytometry identified significantly more B220$^+$ cells in the brains of terminally ill GFAP-LTαβ mice versus NTg (Figures 2C and S2A). IHC revealed large, Myc$^+$, B220$^+$ lymphomas in all regions of GFAP-LTαβ brains, whereas NTg brains exhibited markedly less CNS involvement (Figures 2D–2I and S2B–S2D). GFAP-LTαβ lesions consisted of B220$^+$ cell clusters (Figure 2F) containing lymphoblasts (black arrows in Figures 2E and 2F) often accompanied by erythrocytes (green arrows in Figure 2E), suggesting local BBB disruption. Lesions were found within 5.03 ± 0.85 μm of vessels (red arrows in Figures 2J and 2K), indicating vascular origin. Analysis of GFAP-LTαβ brains infiltrated with E_μ-Myc cells via IHC and qPCR revealed an expression profile consistent with DLBCL, including Myc, IRF4, Bcl2, and immunoglobulin M (Figures S2B–S2F).

To determine whether chronic canonical NF-κB signaling could also promote LC infiltration of the CNS, we administered E_μ-Myc cells to mice in which an inducible, constitutively active (CA) form of IKK2 is expressed under the GFAP promoter ("IKK2CA" mice) (Figure S2G) (Lattke et al., 2012; Oeckl et al., 2012), which we confirmed had intact BBBs prior to lymphoma cell injection (Figure S2H). Similar to GFAP-LTαβ, IKK2CA brains displayed numerous B220$^+$ infiltrates (Figure S2I).

To determine whether neoplastic B cells driven by another oncogene would also invade GFAP-LTαβ or IKK2CA brains, we utilized cells from a different transgenic mouse line overexpressing the T cell leukemia 1 gene in B cells ("E_μ-Tcl1 mice"). E_μ-Tcl1 mice develop chronic lymphocytic leukemia (Bichi et al., 2002) and DLBCLs (Hoyer et al., 2002). Splenocytes from leukemic E_μ-Tcl1 mice were administered i.v. to NTg, GFAP-LTαβ, and IKK2CA mice (Figure 3A). Mice reached terminal disease by 3 months post injection. IHC revealed numerous B220$^+$ infiltrates (Figures 3B, 3C, and S3A) in all regions of GFAP-LTαβ brains, whereas none were identified in NTg (Figure 3D). Many vascular lesions were identified (Figure S3B, left), some of which had disseminated into the surrounding parenchyma (Figure S3B, middle). IKK2CA brains also displayed numerous B220$^+$ infiltrates (Figures 3C and 3D), which were predominantly parenchymal (Figure S3B, right). Brains from E_μ-Tcl1-injected GFAP-LTαβ and IKK2CA mice expressed elevated human *TCL1* (Figure 3E), and immunofluorescence (IF) images of GFAP-LTαβ and IKK2CA brains showed Tcl1-expressing lymphomas (Figure S3C). Therefore, chronic gliosis due to sustained activation of either canonical or alternative NF-κB signaling promotes the infiltration of CNS tissue by diverse neoplastic B cells.

Brains from mice injected with E_μ-Myc or E_μ-Tcl1 LCs exhibited an expression profile consistent with DLBCL (Figures 3F and S3D–S3G), the most common human CNSL subtype. Next, GFAP-LTαβ mice were injected with E_μ-Tcl1 LCs and treated with high-dose methotrexate (HDMTX; Figure S3H). HDMTX treatment resolved all lymphomas (Figures S3I and S3J). Thus, LCs found in the brains of our mice were phenotypically similar to human CNSLs and responded to a common CNSL therapy in the expected manner.

Gliosis Enhances Cell-Adhesion Molecule Expression and LC Entry in the CNS

Next, we investigated the potential role of leukocyte-specific cell-adhesion molecules (CAMs) in gliosis-induced CNSL. *Madcam1*, *Vcam1*, and *Icam1* were elevated in GFAP-LTαβ brains (Figure 4A) in CD31$^+$ endothelial cells (ECs) (Figure 4B). The pan-endothelial marker, *Pecam1* (CD31) and other CAMs implicated in neuroinflammation, including *Mcam*, *Alcam*, and *Selp*, were not elevated (Figure S4A). To demonstrate that NF-κB activation directly influences EC CAM expression, we treated a murine EC line with an LTβR agonistic antibody (ACH6), tumor necrosis factor α (TNFα), or a combination. Maximal elevations of *Madcam1*, *Vcam1*, and *Icam1* were achieved with ACH6 + TNFα (Figure 4C). LFA-1 and VLA-4, the ligands for ICAM1 and VCAM1, are expressed on both E_μ-Myc and E_μ-Tcl1 cells (Heinig et al., 2014; Rehm et al., 2011) (Figures S4B and S4C). To show that NF-κB enhances LC binding to ECs, we incubated E_μ-Myc cells with ACH6-treated ECs. After washing, significantly more E_μ-Myc LCs were bound to ACH6-treated versus untreated ECs (Figures 4D and 4E). We also observed increased E_μ-Myc LCs in GFAP-LTαβ and IKK2CA brains compared with NTg 24 h post injection (Figures 4F–4H). Similarly, significantly more bioluminescence was measured in whole brains of GFAP-LTαβ mice injected with luciferase-expressing E_μ-Myc cells than NTg (Figures 4I and 4J). To determine whether increased LC numbers in GFAP-LTαβ brain were due to enhanced CAM expression on ECs, we treated wild-type (WT) mice with ACH6 prior to administration of E_μ-Myc LCs (Figure 4K; ACH6) and quantified the number of B220$^+$ cells in the brain 24 h later compared with untreated WT (Figure 4F; Ctrl). The effects of ACH6 in the brain should be restricted to the endothelium, since ACH6 cannot penetrate the BBB. ACH6-treated brains upregulated *Icam1* and *Vcam1* (Figure S4D) and contained significantly more LCs than Ctrl (Figures 4L and 4M). To determine whether

(C) Whole-brain fluorescence-activated cell sorting analysis of total B220$^+$ cells per brain in E_μ-Myc-injected NTg and GFAP-LTαβ mice at advanced disease.
(D) Number of mice exhibiting CNS lesions in NTg versus GFAP-LTαβ mice.
(E and F) Brains from terminal NTg and GFAP-LTαβ mice injected with E_μ-Myc LCs were analyzed via H&E (E) or B220 IHC (F). Lymphoblasts (black arrows), erythrocytes (green arrows), cerebellum (CB), forebrain (FB), spinal cord (SC), and meninges (MG). Scale bars, 50 μm.
(G) Number of B220$^+$ cells/lesion. Black bar denotes mean value.
(H) Number of B220$^+$ lesions identified in GFAP-LTαβ versus NTg brain IHC.
(I) Total numbers of B220$^+$ lesions found in different regions of NTg and GFAP-LTαβ brains.
(J) H&E of brain from terminal GFAP-LTαβ mouse injected with E_μ-Myc LCs. Red arrows indicate blood vessels. Scale bar, 100 μm (inset, 50 μm).
(K) CoIF of CNSL in GFAP-LTαβ brain. CD45.2 (red), CD31 (green), DAPI (blue). Scale bar, 100 μm.
All error bars denote SEM. See also Figure S2. *$p < 0.05$, **$p < 0.01$, ***$p < 0.001$.

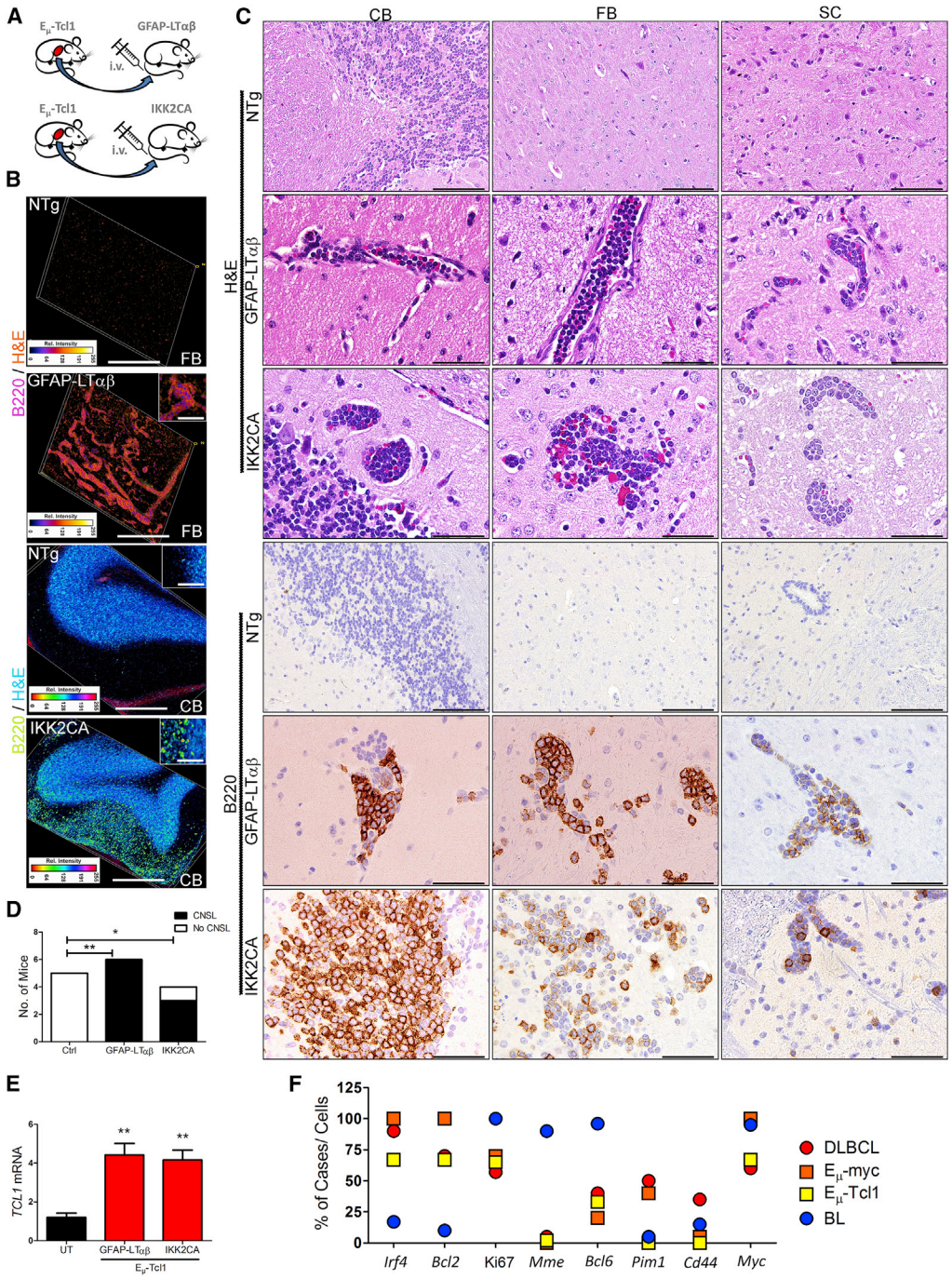

Figure 3. Chronic Gliosis Promotes the Formation of E_μ-Tcl1 Lymphomas in the CNS

(A) GFAP-LTαβ, IKK2CA, and NTg mice were injected i.v. with E_μ-Tcl1 splenocytes and sacrificed at terminal disease.

(B) 3D reconstructions of stacked B220 images from NTg, GFAP-LTαβ, and IKK2CA brains. Scale bars, 200 μm (insets, 50 μm).

(C) H&E and B220 IHC of brains from NTg, GFAP-LTαβ, and IKK2CA mice injected with E_μ-Tcl1 cells at terminal disease. Cerebellum (CB), forebrain (FB), and spinal cord (SC). Scale bars 100 μm (NTg) and 50 μm (GFAP-LTαβ, IKK2CA).

(D) The number of NTg (Ctrl), GFAP-LTαβ, and IKK2CA mice injected with E_μ-Tcl1 cells with $B220^+$ brain lesions (CNSL).

(E) Expression of human *TCL1* in the brains of E_μ-Tcl1-injected GFAP-LTαβ and IKK2CA versus untreated GFAP-LTαβ mice (UT) via qPCR. Error bars denote SEM.

(F) mRNA or protein (Ki67) expression profile of E_μ-Myc and E_μ-Tcl1 brain lesions compared with human DLBCL and Burkitt lymphoma (BL), another Myc-driven malignancy. n = 5 mice per group. Human DLBCL and BL numbers are based on published data (see, e.g., Bellan et al., 2009; Dave et al., 2006; Deckert et al., 2014a, 2014b; Harris et al., 2001; Hochberg et al., 2007; Nasr et al., 2010; Nawijn et al., 2011).

See also Figure S3. *p < 0.05, **p < 0.01, ***p < 0.001.

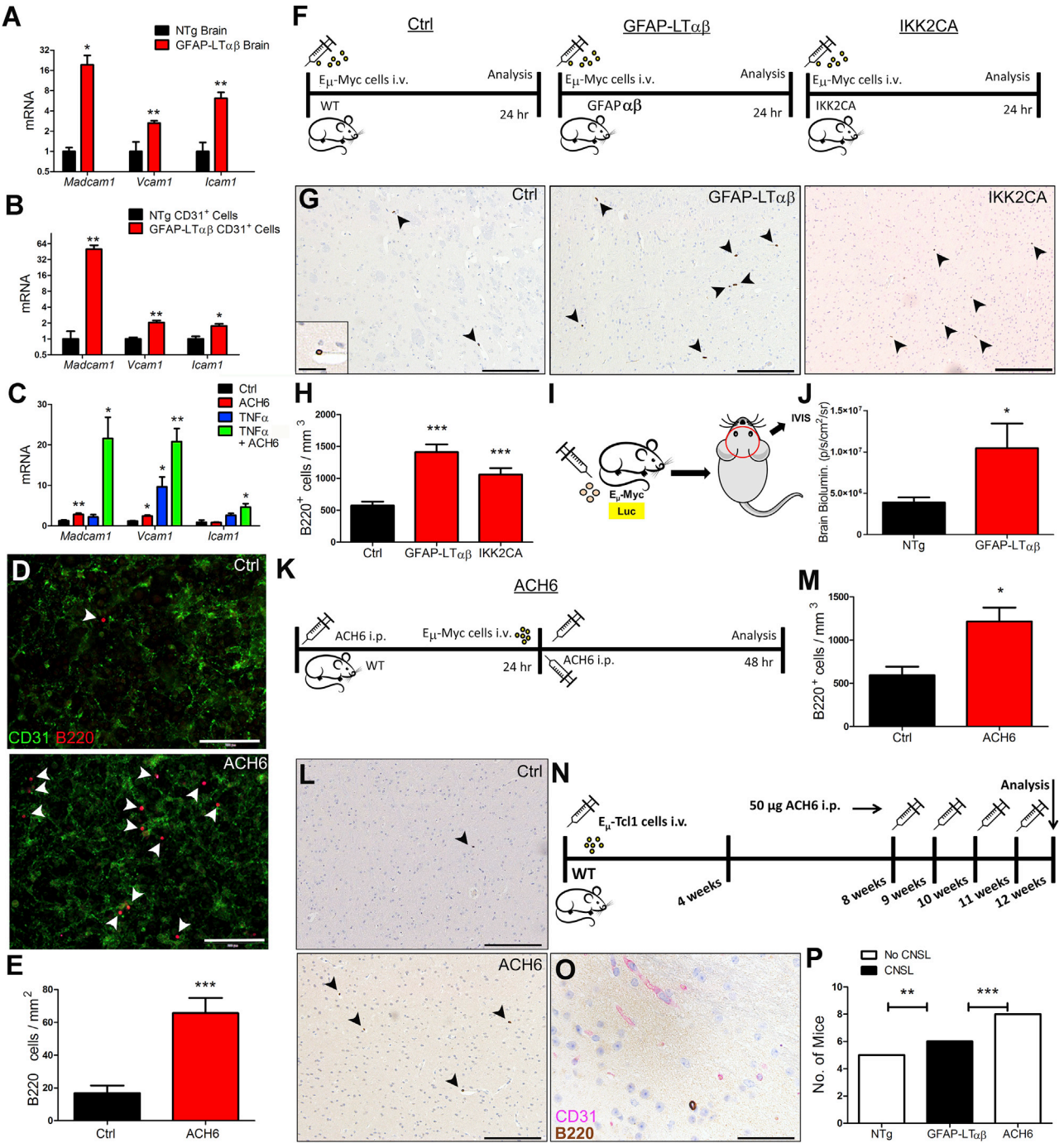

Figure 4. Upregulated Leukocyte-Specific Adhesion Molecules on Brain Endothelium Increases Steady-State LC Numbers in the Brain But Does Not Induce CNS Lymphomas

(A and B) qPCR analysis of *Icam1*, *Madcam1*, and *Vcam1* mRNAs in NTg or GFAP-LTαβ brains (A) or $CD31^+$ cells isolated from NTg and GFAP-LTαβ brains (B). n = 5 per group.

(C) qPCR analysis of *Icam1*, *Madcam1*, and *Vcam1* expression in a murine endothelial cell line (EC) either untreated (Ctrl) or treated for 16 h with ACH6, TNFα, or TNFα + ACH6.

(D) ECs were either untreated (Ctrl) or treated for 16 h with ACH6 and incubated for 1 h with E_μ-Myc LCs, then stained with CD31 (green) and B220 (red). Scale bars, 100 μm. n = 6 wells per treatment.

(E) The number of $B220^+$ cells per mm^2 in (D).

(F) WT (Ctrl), GFAP-LTαβ, or IKK2CA mice were injected i.v. with E_μ-Myc LCs and sacrificed at 24 h.

(G) B220 IHC of brains from (F). Black arrows indicate $B220^+$ cells. Scale bars, 200 μm (inset, 25 μm). n = 5–8 mice per group.

(legend continued on next page)

brain CAM upregulation was sufficient for CNSL formation, we administered ACH6 weekly to WT mice that had been injected with E_μ-Tcl1 LCs 1 month prior to terminal disease (Figure 4N). Brains from ACH6-treated mice upregulated *Icam1* and *Vcam1* (Figure S4E) and contained isolated parenchymal LCs (Figure 4O) but exhibited no CNSL (Figure 4P). Thus, CAM upregulation alone appears to be insufficient to induce CNSL.

Chronic Gliosis Increases the Number of Parenchymal LCs without Affecting Proliferation

We next considered the possible role of chemokines in gliosis-induced CNSL. WT brains expressed negligible *Ccl19*, *Ccl21*, and *Cxcl13* and high *Cxcl12* compared with spleen (Figure 5A). *Cxcl13*, *Ccl19*, and *Ccl21* were elevated in GFAP-LTαβ brains, and *Cxcl12* was unaltered (Figure 5B). To determine the percentage of vascular ($CD31^+$) versus parenchymal ($CD31^-$) LCs, we performed B220/CD31 co-IHC on Ctrl, ACH6, and GFAP-LTαβ brains from Figures 4F and 4K (Figure 5C). The total number of LCs was significantly higher in ACH6-treated brains compared with Ctrl (Figure 5D, red); however, the ratio of parenchymal to vascular LCs was similar (Figure 5E). In contrast, GFAP-LTαβ brains contained significantly more total parenchymal LCs (Figure 5D, red) and a significantly higher ratio of parenchymal to vascular LCs compared with Ctrl and ACH6 (Figure 5E). Surprisingly, 51% of LCs were in the parenchyma of untreated WT brains at 24 h (Figure 5E), indicating that LCs enter the brain parenchyma even in the absence of gliosis. A time-course study of LC injections in WT mice showed that 12% of LCs were in the brain parenchyma by 5 min post injection (Figure 5F), which increased over 24 h. Total LCs in the brain remained relatively stable (Figure 5F, red line). To confirm this observation using an independent method, we performed two-photon microscopy (2PM) on WT animals fitted with a cortical glass window and injected them i.v. with fluorescein isothiocyanate (FITC)-labeled dextran and CellTracker red (CMTPX)-labeled E_μ-Myc cells (Figure 5G). We observed LCs in vessels, extravasating LCs, and LCs that had already extravasated in WT and GFAP-LTαβ brains at 2, 24, and 48 h post injection (Figures 5H and Figures S5A–S5C). The number of parenchymal LCs in GFAP-LTαβ brains was significantly higher than in WT (Figure 5I). Survival factors from GFAP-LTαβ astrocytes could explain the higher frequency of LCs in GFAP-LTαβ brains. However, the viability and proliferation rates of E_μ-Myc cells in media conditioned by NTg versus GFAP-LTαβ primary glia were similar (Figure 5J). Moreover, E_μ-Myc cells survived up to 60 h without serum (Figure 5K). Finally, E_μ-Myc lymphomas transplanted into WT brains grew over time (Figure 5L). Therefore, E_μ-Myc LCs are, in principle, capable of proliferating in WT brains.

LCs Are Retained in the Brain Parenchyma at a Higher Frequency during Gliosis

LCs were capable of entering and proliferating in WT brains. However, CNSL rarely formed in WT brains when administered i.v. To find an explanation for this, we traced the fates of individual LCs in WT and GFAP-LTαβ brains over 48 h with 2PM. Vascular LCs tended to be transient in both genotypes (Figures 6A, 6B, 6C, S6A, and S6B). However, parenchymal LCs were retained at a significantly higher rate in GFAP-LTαβ brains compared with WT (Figures 6A, 6B, 6C, S6A, and S6B). Moreover, LCs accumulated over time in GFAP-LTαβ brains (Figure 6D). LC proliferation was observed only once in WT brain (Figure S6C). LCs were always spatially separated, again arguing against proliferation (Figure S6D). Endothelial CXCL12 has been reported to limit parenchymal dissemination of immune cells in the brain (McCandless et al., 2006). We also observed endothelial CXCL12 in WT brain (Figures S6E and S6F). Moreover, E_μ-Myc cells express CXCR4 (Figure S6G). We therefore theorized that in WT brains, parenchymal LCs re-enter the vasculature within a time frame inconsistent with mature tumor growth due to endothelial CXCL12 (Figure 6E). In GFAP-LTαβ brains, LCs might be retained in the parenchyma for a longer period of time by a chemokine produced by activated glia, thereby increasing the likelihood of tumor formation. However, the majority of LCs most likely eventually leave GFAP-LTαβ brains via the same mechanism. In support of this hypothesis, we observed single LCs re-entering the brain vasculature in both GFAP-LTαβ (Figure 6F) and WT brains (Figures 6G, 6H, and S6H; Videos S1, S2, and S3) by single cell tracing.

Formation of Gliosis-Induced CNSL Requires CCL19-CCR7 Signaling

To identify the putative parenchymal chemokine retaining LCs in GFAP-LTαβ brains, we analyzed chemokine expression in GFAP-LTαβ brains from which the vessel-rich meninges had been removed. Significantly reduced *Cxcl13* and *Ccl21* were observed in GFAP-LTαβ brains without meninges (Figure 7A), indicating that these chemokines were mainly produced in the vasculature. Moreover, IKK2CA brains lack *Cxcl13* and *Ccl21* mRNA (Table S1), and E_μ-Myc cells lack CXCR5 (Figure S7A). In contrast, *Ccl19* mRNA remained high in GFAP-LTαβ brains without meninges (Figure 7A), and both E_μ-Myc (Figure S7B) and E_μ-Tcl1 cells (Heinig et al., 2014) express CCR7. Thus, we considered CCL19 to be the most likely chemokine mediating

(H) The total number of $B220^+$ cells per mm^3 in (G) was quantified and averaged for n = 5 mice per treatment group.
(I) NTg or GFAP-LTαβ mice were injected i.v. with luciferase-expressing E_μ-Myc LCs and intraperitoneally (i.p.) with luciferin, and the total amount of *in vivo* bioluminescence (IVIS) was quantified.
(J) IVIS measurements of mice in (I) in photons per second per cm^2 per steradion (p/s/cm^2/sr). n = 9–10 mice per group.
(K) WT mice were injected i.p. with ACH6 24 h prior to, as well as simultaneously with, administration of E_μ-Myc LCs i.v. n = 5 mice per group.
(L) B220 IHC of brains in (K). Scale bars, 200 μm.
(M) Quantification of brains in (K).
(N) WT animals were injected with E_μ-Tcl1 LCs. One month prior to terminal disease, mice were treated weekly with ACH6. n = 8 mice.
(O) B220/CD31 co-IHC (B220 = brown, CD31 = pink) of brains from (N). Scale bar, 50 μm.
(P) Incidence of CNSL in mice from (N) compared with E_μ-Tcl1-injected NTg or GFAP-LTαβ mice at terminal disease.
All error bars denote SEM. See also Figure S4. *p < 0.05, **p < 0.01, ***p < 0.001.

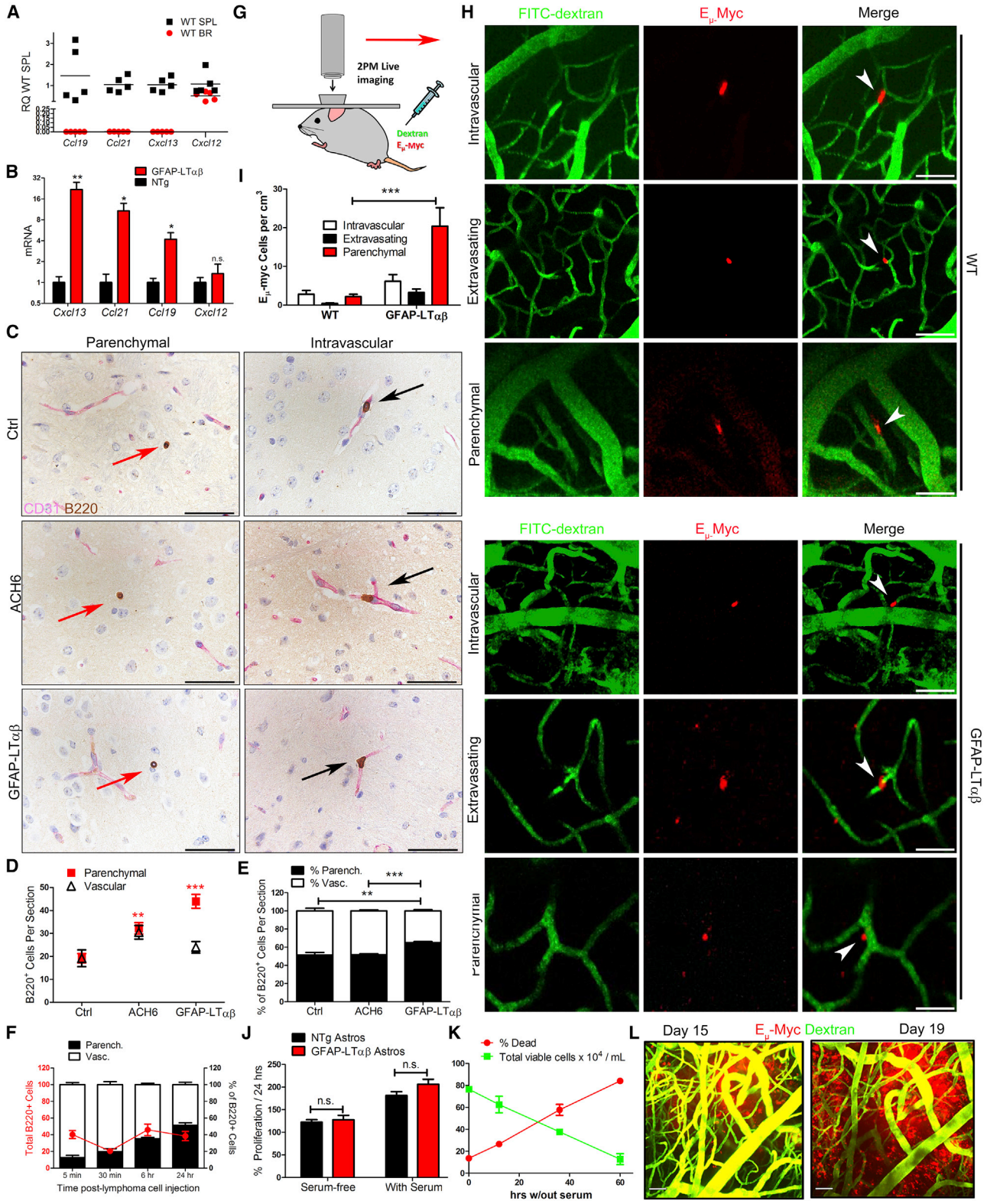

Figure 5. Chronic Gliosis Increases the Number of Parenchymal LCs without Affecting Proliferation

(A and B) qPCR of *Ccl19*, *Ccl21*, *Cxcl13*, or *Cxcl12* in WT brain (BR) versus WT spleen (SPL) (A) or in NTg or GFAP-LTαβ brains (B). n = 5 mice per group. Black lines denote mean values.

(legend continued on next page)

parenchymal retention of LCs. Accordingly, IKK2CA brains also expressed *Ccl19* in a transgene-dependent manner (Figure S7C). Moreover, GFAP-LTαβ primary astrocytes expressed significantly more *Ccl19* than NTg (Figure 7B), and stimulation of either canonical or non-canonical NF-κB signaling in WT astrocytes elevated *Ccl19* mRNA (Figure S7D) and protein (Figure S7E). IF of GFAP-LTαβ and IKK2CA brains identified CCL19$^+$ astrocytes (Figures 7C and 7D), and confocal analysis of TNFα + ACH6-treated astrocytes revealed cell-surface and endocytic CCL19 protein (Figures S7F and S7G). To determine whether CCL19 was required in the brain and CCR7 was required on LCs for CNSL formation, we administered *Ccr7*$^{-/-}$ E_μ-Myc cells to GFAP-LTαβ or IKK2CA mice and E_μ-Myc cells to GFAP-LTαβ × plt/plt mice (lacking CCL19) and analyzed their brains at terminal disease (Figures 7E and S7H). The ability of *Ccr7*$^{-/-}$ LCs to form lesions within GFAP-LTαβ (Figures 7F–7H) and IKK2CA brains (Figures S7I and S7J) was significantly reduced, although *Ccr7*$^{-/-}$ LCs could enter the brain parenchyma (Figure S7K). GFAP-LTαβ × plt/plt mice injected with E_μ-Myc LCs also failed to form CNSL (Figures 7F–7H). To show that CCL19 counteracts the effects of CXCL12 on LCs, we performed an *in vitro* transwell experiment (Figure 7I). CXCL12 induced migration of up to 4% of E_μ-Myc cells over 24 h (red line in Figures 7J and S7L), and CCL19 significantly counteracted this effect (green line in Figure 7J). CCL19 had no effect on the migratory behavior of *Ccr7*$^{-/-}$ E_μ-Myc cells toward CXCL12 (Figure 7J), and CCL19 did not affect proliferation of E_μ-Myc cells over 24 h (Figure S7M). *Cxcr4*$^{-/-}$ E_μ-Myc cells displayed reduced brain infiltration (Figure 7K), confirming that CXCL12 is involved in LC brain extravasation. To determine how lacking CCR7 would affect LC behavior in GFAP-LTαβ brain, we administered *Ccr7*$^{-/-}$ E_μ-Myc cells to GFAP-LTαβ mice and traced the fate of *Ccr7*$^{-/-}$ E_μ-Myc cells over 48 h. In contrast to normal E_μ-Myc cells, *Ccr7*$^{-/-}$ E_μ-Myc cells were retained in GFAP-LTαβ brains at a significantly lower frequency (Figures 7L and 7M). Thus, CCL19 produced by astrocytes and CCR7 expressed by LCs appear to be required for gliosis-induced retention of LCs observed in GFAP-LTαβ brains.

Evidence for a CCL19-Retention Mechanism in Age-Related Gliosis

Next, we tested for expression of inflammatory mediators in human PCNSL and SCNSL surgical biopsies and identified a number of upregulated NF-κB signaling components (Figures 8A and S8A). To distinguish between NF-κB targets expressed by lymphoma versus brains cells, we performed a linear regression analysis of NF-κB target genes versus the corresponding *CD20* expression in the same sample. *A20*, *LTA*, *LTB*, *TNFA*, *NFKB1*, and *NFKB2* were correlated with CD20 (Figure S8A), whereas *CCL19*, *CCL21*, *CXCL13*, *VCAM1*, and *ICAM1* were not (Figure S8B), indicating that expression of the latter might emanate from brain cells. *CCR7* was also significantly correlated with *CD20* in PCNSL and SCNSL patients (Figure S8B), and CCR7$^+$ LCs were identified by IF (Figure S8C). Some PCNSL and SCNSL patients also exhibited elevated CCL19 in cerebrospinal fluid (CSF) (Figure 8B). Consistent with the idea that gliosis could be a pre-existing condition promoting CNSL, we also detected elevated expression of inflammatory genes (Figure S8D) and CCL19 in gliosis brains (Figures 8C–8E). Gliosis incidence increases with age, and the average age of onset for PCNSL is ~65 years (Bessell et al., 2011). To show that age-related gliosis could be a risk factor for developing CNSL, we compared the ability of CNSL to form in the brains of 2-month-old versus 11-month-old WT mice injected with E_μ-Myc LCs (Figure 8F). Consistent with our hypothesis, aged mice with gliosis developed significantly larger B220$^+$ lesions in the brain than young mice (Figures 8G and 8H). Eleven-month-old brains expressed significantly more GFAP protein (Figures 8I and 8J), as well as markers of myeloid cell activation and enhanced antigen presentation (Figures 8K and 8L). Elevated CCL19 protein was detected in 11-month-old mouse brains via IF (Figures S8E and S8F) and ELISA (Figure S8G). Moreover, mass spectrometry-based proteomic comparison of 11-month-old versus 2-month-old brains revealed enrichment of proteins involved in several inflammatory pathways in aged brains (Figure S8H), many of which were held in common with GFAP-LTαβ brains, albeit on a less pronounced scale (Figures S8I–S8K). Therefore, evidence for the CCL19-CCR7 retention mechanism identified in GFAP-LTαβ brains exists in human gliosis and CNSL patients, and age-related gliosis significantly increases the risk of developing CNSL.

DISCUSSION

Here, we describe a mechanism that enables LC retention in the brain and formation of CNSL. Circulating LCs were fully capable

(C) CD31 (pink) and B220 (brown) co-IHC of brains from Figures 4F and 4K. Right images: vascular B220$^+$ cells (black arrows). Left images: parenchymal B220$^+$ cells (red arrows). Scale bars, 50 μm.
(D and E) Total numbers (D) and the ratio (E) of parenchymal versus vascular LCs in (C). n = 5 mice per group.
(F) Ratio of parenchymal (black) versus vascular (white), and total (red line) B220$^+$ cells in WT mice 5 min, 30 min, 6 h, and 24 h after i.v. injection with E_μ-Myc LCs. n = 5 mice per group.
(G) Mice were injected i.v. with FITC-dextran and CMTPX (red)-labeled E_μ-Myc LCs and used for two-photon (2PM) microscopic analysis of the brain up to 500 μm into the cortex.
(H) 2PM *in vivo* images of FITC-dextran (green)-labeled vessels and CMTPX (red)-labeled E_μ-Myc cells in vessels (intravascular; z = 30–90 μm WT; 25–95 μm GFAP-LTαβ), extravasating (z = 60–120 μm WT; 420–460 μm GFAP-LTαβ), or parenchymal (z = 15–75 μm WT; 225–245 μm GFAP-LTαβ) in WT and GFAP-LTαβ brains. Scale bars, 20 μm.
(I) LC distribution at 48 h post injection from 2PM live images in GFAP-LTαβ and WT brains.
(J) Proliferation rate of E_μ-Myc LCs incubated in complete (with serum) or serum-free medium conditioned for 24 h by NTg or GFAP-LTαβ primary astrocytes.
(K) Death rate (red line) and proliferation rate (green line) of E_μ-Myc cells without serum.
(L) Transplantation of E_μ-Myc cells into WT brain and 2PM imaging at day 15 (x × y × z dimensions = 443 μm × 377 μm × 250 μm) and day 19 (x × y × z dimensions = 488 μm × 448 μm × 280 μm) post transplantation. Scale bars, 50 μm.
All error bars denote SEM. See also Figure S5. *p < 0.05, **p < 0.01, ***p < 0.001.

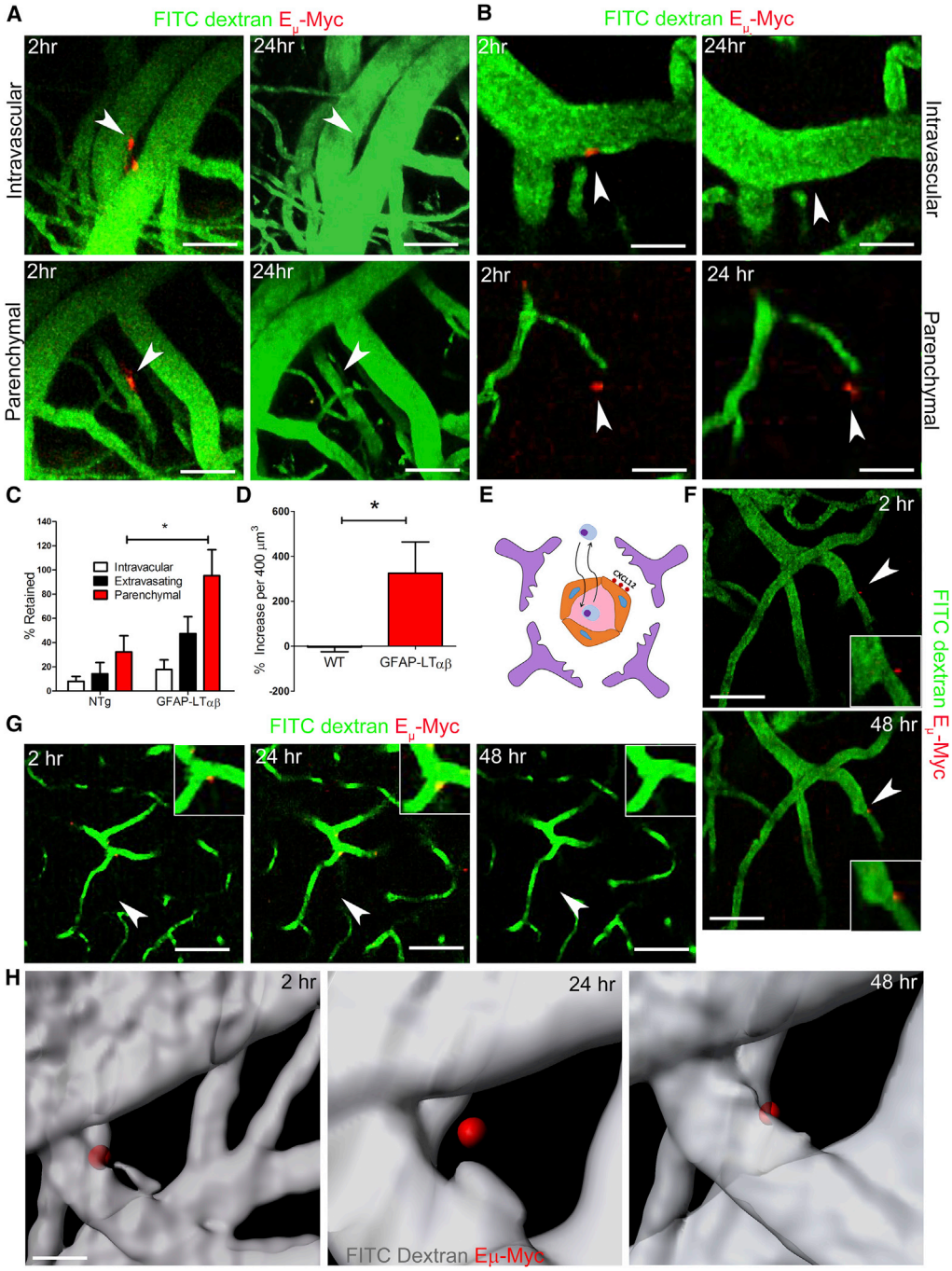

Figure 6. Parenchymal LCs Are Retained at a Higher Rate in Brains with Chronic Gliosis

(A and B) 2PM time-lapse imaging of individual LCs over 24 h in WT (A) and GFAP-LTαβ (B) brains. Vascular LCs (upper images; z = 15–75 μm WT; z = 4–19 μm GFAP-LTαβ); parenchymal cells (lower images; z = 10–60 μm WT; 230 μm GFAP-LTαβ). Scale bars, 50 μm.

(C) Percentage of intravascular (white), extravasating (black), and parenchymal (red) LCs retained from 24 to 48 h in WT versus GFAP-LTαβ brains.

(D) Percent increase in total LCs in WT versus GFAP-LTαβ brains over 24 h per cm^3.

(E) Proposed model of LC behavior in WT brains: LCs enter the brain parenchyma transiently due to high endothelial CXCL12.

(F) 2PM time-lapse imaging of a GFAP-LTαβ brain showing a parenchymal LC at 2 h re-entering the vasculature at 48 h (white arrows; z = 50 μm.). Scale bars, 100 μm.

(G) 2PM time-lapse imaging of a WT brain showing an extravasating LC at 2 h fully re-entering the vasculature by 24 h and disappearing by 48 h (white arrows; z = 380 μm). Scale bars, 100 μm.

(H) 3D reconstructions of 2PM time-lapse images of an LC extravasating at 2 h, in WT brain parenchyma at 24 h, and re-entering the vasculature by 48 h. Scale bar, 10 μm.

All error bars denote SEM. See also Figure S6; Videos S1, S2, and S3. *p < 0.05, **p < 0.01, ***p < 0.001.

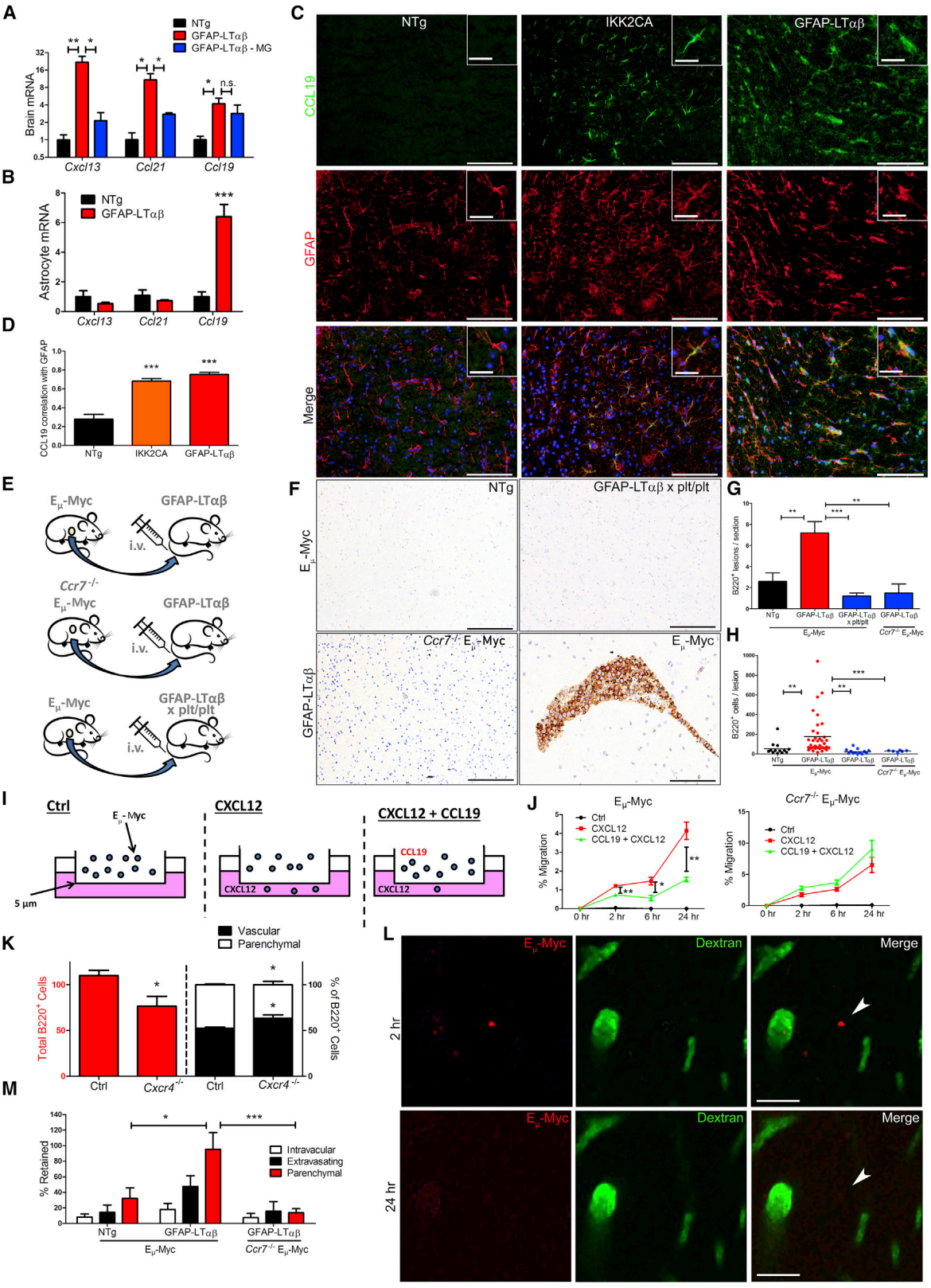

Figure 7. Astrocytic CCL19 and CCR7 on LCs Are Required for Gliosis-Induced B Cell Lymphomas in the CNS

(A) qPCR of *Ccl19*, *Ccl21*, or *Cxcl13* mRNA in NTg, GFAP-LTαβ, or GFAP-LTαβ brains from which the meninges (MG) had been removed.

(B) qPCR of *Cxcl13*, *Ccl21*, and *Ccl19* mRNA in NTg versus GFAP-LTαβ primary astrocytes.

(legend continued on next page)

of entering the brain parenchyma, but only transiently, presumably re-entering the vasculature due to endothelial CXCL12 (McCandless et al., 2006). The rate of LC movement between the brain parenchyma and the vasculature was intermediate between what has been reported for T lymphocytes, which extravasate within minutes (Schlager et al., 2016), and non-lymphocytic cancer cells, which can take days (Kienast et al., 2010). NF-κB activation stimulated CCL19 production in astrocytes, and CCL19 counteracted the migratory effect of CXCL12 on LCs. *In vivo*, this resulted in significantly enhanced parenchymal retention of LCs. Enhanced parenchymal LC retention in gliotic brains elevated the risk of forming CNSL. Whether CCL19-mediated retention affects the ability of other cancer cell types to extravasate in the brain remains unknown. However, given the established role of chemokines in metastasis, it seems plausible that similar mechanisms might operate within the brain. Additional mechanisms may also contribute to LC parenchymal retention, such as antigen recognition (Montesinos-Rongen et al., 2015). Antigen- and CCL19-mediated parenchymal retention are not necessarily mutually exclusive. Elevated MHCII expression was found in GFAP-LTαβ meninges, which could enhance antigen presentation to and activation of circulating LCs. Moreover, antigen engagement of LCs might increase CCR7 expression. Vascular CXCL13 was also elevated in GFAP-LTαβ brains, which was the likely reason for vascular lesions in GFAP-LTαβ brains infiltrated with CXCR5$^+$ E_μ-Tcl1 cells. However, CXCL13 and CXCR5 were not required for gliosis-induced CNSL. Specific chemokine expression profiles in individual brains, as well as the chemokine receptor expression of circulating transformed B cells, will likely determine the probability that LCs enter the brain parenchyma, since cell-surface expression of CXCR5 and CCR7 vary during B cell maturation (Bowman et al., 2000) and among B cell malignancies (Wong and Fulcher, 2004). Since T cells express CCR7, gliosis might also promote CNS T cell malignancies. Accordingly, it has been reported that CCR7 is important for CNS involvement in T cell acute lymphoblastic leukemia (Buonamici et al., 2009).

CNS lymphomas predominantly display an ''activated B cell'' (ABC) phenotype (Bhagavathi et al., 2008; Camilleri-Broet et al., 2006; Cheng et al., 2008; Hattab et al., 2010; Mahadevan et al., 2015). This phenomenon may be related to CCR7 expression, as ABCs upregulate CCR7 to migrate to the T cell zone of lymphoid organs (Reif et al., 2002). Moreover, it raises the question of whether cancer therapies blocking lymphocyte activation might also be useful for CNSL. In support of this idea, it has been reported that an inhibitor of B cell receptor downstream signaling, ibrutinib, is effective for the treatment of PCNSL (Choquet et al., 2016; Lionakis et al., 2017). Thus, in addition to the accumulation of particular BCR-related co-mutations (Phelan et al., 2018; Wilson et al., 2015) and resistance mutations (Grommes et al., 2017), the effectiveness of ibrutinib in the CNS might also be related to selective retention of LCs with activated BCR signaling due to higher CCR7 levels.

We have developed a non-surgical model of CNSL with an intact BBB in immunocompetent mice, which may be used to investigate mechanisms of lymphoma cell entry in the brain at the earliest stages of CNSL or to test strategies for preventing SCNSL. Moreover, we identified CCL19-expressing astrocytes in both human CNSL and gliosis. GFAP-LTαβ and IKK2CA CNSL were phenotypically similar to human CNSL and responded to a common CNSL therapy (HDMTX) in the expected manner, corroborating the validity of our models. Finally, we showed experimentally that age-related gliosis alone can directly influence the formation of CNSL, demonstrating that chronic gliosis could, in principle, be a driving factor in human CNSL. Elevated CCL19 has been reported in the CNS during MS (Krumbholz et al., 2007), including in astrocytes (Columba-Cabezas et al., 2003). TLOs, the manifestation of chronic ectopic NF-κB activation, are often found in nervous tissue in chronic demyelinating disorders. A number of studies have reported histologically confirmed demyelinating lesions in the brains of patients that later developed PCNSL (Alderson et al., 1996; Husseini et al., 2012; Lu et al., 2016; Lyons et al., 2011). PCNSL has an average age of onset of 65 years in immunocompetent individuals (Bessell et al., 2011), and chronic gliosis is a general feature of aging brains, including upregulated NF-κB-related cytokines, such as TNFα and IL-6 (Lynch et al., 2010). Increased age is known to be a factor contributing to increased risk for lymphoma dissemination to the CNS (Tomita et al., 2018). Interestingly, 81% of relapsed PCNSL lesions occur in a spatially distinct location from the original lesion (Ambady et al., 2017), which might be explained by a pre-existing condition, such as gliosis, in the brain. Thus, in addition to other known molecular mechanisms driving CNSL pathogenesis, such as general increased lymphoma risk with age (Chapuy et al., 2018) and immune evasion (Nayak et al., 2017), age-related gliosis and astrocytic CCL19 may also be important factors determining overall risk for CNSL.

(C) IF of NTg, IKK2CA, and GFAP-LTαβ brains for CCL19 (green), GFAP (red), and DAPI (blue). Scale bars, 100 μm (insets, 25 μm).
(D) Quantification of the degree of correlation between CCL19 and GFAP immunosignals in IKK2CA and GFAP-LTαβ brains versus NTg.
(E) E_μ-Myc or *Ccr7*$^{-/-}$ × E_μ-Myc cells were injected i.v. into GFAP-LTαβ or GFAP-LTαβ × plt/plt mice. n = 5–10 mice per group.
(F) B220 IHC of brains from (E). Scale bars, 100 μm except for GFAP-LTαβ (50 μm).
(G and H) B220$^+$ lesions per brain section (G) and B220$^+$ cells per lesion (H) from brains in (E).
(I) Transmigration assays with LCs in the upper chamber (Ctrl), LCs in the upper chamber with CXCL12 in the lower chamber (CXCL12), or LCs co-incubated with CCL19 in the upper chamber and CXCL12 in the lower chamber (CXCL12 + CCL19).
(J) Percentage of E_μ-Myc or *Ccr7*$^{-/-}$ E_μ-Myc LCs in the lower chamber at 2, 6, and 24 h.
(K) E_μ-Myc (Ctrl) or *Cxcr4*$^{-/-}$ E_μ-Myc cells (1×10^6) were injected i.v. into WT mice, and total numbers of B220$^+$ cells as well as the percentage of E_μ-Myc cells in the brain parenchyma versus the vasculature was evaluated 24 h post injection via IHC. n = 5 mice per group.
(L) 2PM time-lapse imaging over 24 h of GFAP-LTαβ mice injected with *Ccr7*$^{-/-}$ E_μ-Myc cells (red); z = 66–78 μm. Scale bars, 30 μm.
(M) Percentage of E_μ-Myc LCs retained from 24 to 48 h in NTg or GFAP-LTαβ brains versus *Ccr7*$^{-/-}$ E_μ-Myc LCs in GFAP-LTαβ brains as determined by 2PM.
All error bars denote SEM. See also Figure S7 and Table S1. *$p < 0.05$, **$p < 0.01$, ***$p < 0.001$.

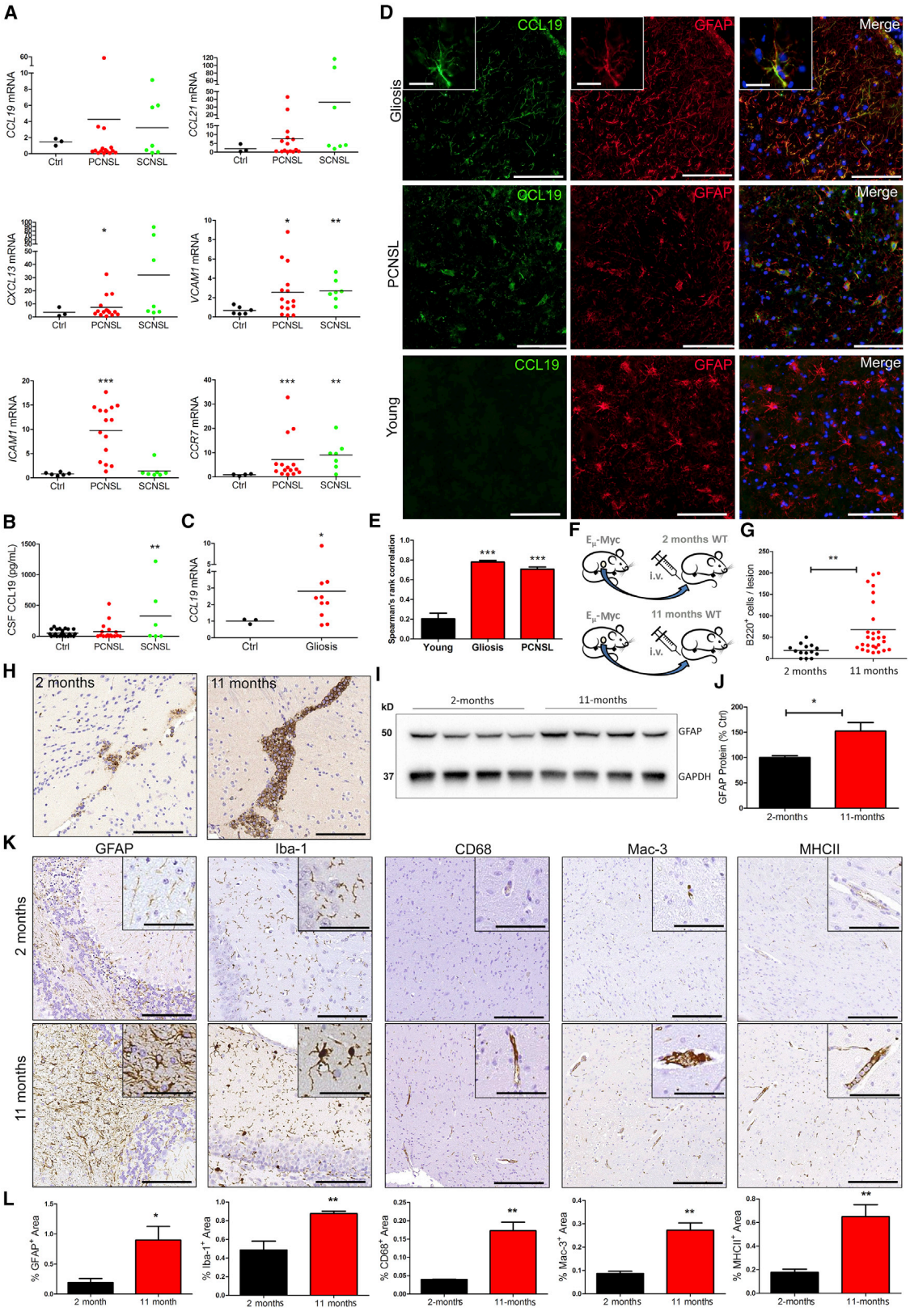

(legend on next page)

STAR★METHODS

Detailed methods are provided in the online version of this paper and include the following:

- KEY RESOURCES TABLE
- LEAD CONTACT AND MATERIALS AVAILABILITY
- EXPERIMENTAL MODEL AND SUBJECT DETAILS
  - GFAP-LTαβ Mice
  - GFAP-tTA-IKK2CA Mice
  - Plt Mice
  - Aged Mice
  - "Primary" E_μ-Myc Lymphoma Cells
  - "Primary" E_μ-Tcl1 Lymphoma Cells
  - *Ccr7*$^{-/-}$ E_μ-Myc Cells
  - Primary Glia Cultures
  - E_μ-Myc "665" Lymphoma Cell Line
  - sEnd.1 Cell Line
  - Human Samples
- METHOD DETAILS
  - Animals and Treatments
  - Brain Cell Isolation
  - Mass Spectrometry-Based Proteomics analysis
  - Cell Culture
  - FACS
  - Immunocytochemistry
  - Real Time PCR
  - LTα ELISA
  - CCL19 ELISA
  - Immunohistochemistry, Quantifications, and 3D Reconstructions
  - Immunofluorescence and Quantifications
  - Western Blots and Cytokine Arrays
  - Analyzing Blood Brain Barrier Integrity
  - *In Vivo* Bioluminescence
  - *In Vivo* Two-Photon Microscopy
- QUANTIFICATION AND STATISTICAL ANALYSIS
- DATA AND CODE AVAILABILITY

SUPPLEMENTAL INFORMATION

Supplemental Information can be found online at https://doi.org/10.1016/j.ccell.2019.08.001.

ACKNOWLEDGMENTS

Funding: T.O., DFG #5892/5-1; M.H., Helmholtz Preclinical Comprehensive Cancer Center (PCCC), ERC Starting (LiverCancerMechanisms) and Consolidator (HepatoMetaboPath) grants, the Stiftung für biomedizinische Forschung, and SFBTR179, 209, and 1335; U.K., Deutsche Krebshilfe #111305 and 111944, DFG SFB824, and the Helmholtz-Gemeinschaft, Zukunftsthema "Immunology and Inflammation" (ZT-0027); L.B., Else Kröner-Fresenius-Stiftung, grant 2014_A265, Bayerische Gleichstellungsförderung der LMU, and Förderprogramm für Forschung und Lehre der LMU, grant 863; R.S., Berta-Ottenstein-Programme; F.M., SFB 1335, BMBF 031B0686B; A.S., ALTF 539-2018. We thank P. Pelczar, M. Delic, T. Sijmonsma, J. Biebl, O. Seelbach, J. Hetzer, R. Hillermann, M. Wimmer, U. Rothermel, H. Fleige, S. Gaupp, C. Gropp, A. Jacob, F. Müller, R. Zeiser, and P. Matei for excellent scientific support.

AUTHOR CONTRIBUTIONS

Conceptualization, T.O., A. Adili, B.S., B.B., A. Aguzzi, U.E.H., U.K., and M.H.; Methodology, T.O., A. Adili, J.K., M.S., B.H, K.M., M.M., B.S., D.W., M.A., D.I., A.H., M.P., E.K., L.v.B., U.E.H., U.K., X.Z., P.A.K., M.G.B., F.M., A.S., N.D., D.P., E.K., and M.H.; Investigation, T.O., X.Z., A. Adili, J.K., M.G.B., B.H., D.H., K.M., E.K., D.W., W.Z., M.A., A.-L.J., M.S., M.M., P.W., G.S., J.B., N.D., D.P., and A.S.; Resources, M.S., M.M., R.S., A.H., T.W., M.P, B.B., A. Aguzzi, L.v.B., U.E.H., U.K., P.A.K., A.W., R.H., U.P., H.A., S.B., F.S., U.K., and M.H.; Writing, T.O.; Editing, U.K. and M.H.; Funding Acquisition, T.O. and M.H.

DECLARATION OF INTERESTS

The authors declare no competing interests.

Received: December 9, 2018
Revised: June 5, 2019
Accepted: August 5, 2019
Published: September 16, 2019

REFERENCES

Adams, J.M., Harris, A.W., Pinkert, C.A., Corcoran, L.M., Alexander, W.S., Cory, S., Palmiter, R.D., and Brinster, R.L. (1985). The c-myc oncogene driven by immunoglobulin enhancers induces lymphoid malignancy in transgenic mice. Nature *318*, 533–538.

Alderson, L., Fetell, M.R., Sisti, M., Hochberg, F., Cohen, M., and Louis, D.N. (1996). Sentinel lesions of primary CNS lymphoma. J. Neurol. Neurosurg. Psychiatry *60*, 102–105.

Alessandro, L., Pastor Rueda, J.M., Villalonga, J.F., Bruno, V.A., Carpani, F., Blaquier, J.B., Tognarelli, S., Varela, F.J., and Muggeri, A. (2017).

Figure 8. Evidence for a CCL19-CCR7 Retention Mechanism in Age-Related Gliosis

(A) *CCL19*, *CCL21*, *CXCL13*, *VCAM1*, *ICAM1*, and *CCR7* mRNA level in human primary central nervous system lymphoma (PCNSL) and secondary central nervous system lymphoma (SCNSL) compared with those in unaffected brain (Ctrl).
(B) CCL19 protein levels in CSF from PCNSL or SCNSL patients or healthy (Ctrl) individuals were measured via ELISA.
(C) *CCL19* mRNA in brain biopsies from humans with gliosis compared with that in unaffected control (Ctrl).
(D) IF of brain sections from human gliosis, PCNSL patients, or young controls for CCL19 (green) and GFAP (red). Blue, DAPI. Scale bars, 100 μm (insets, 25 μm).
(E) Quantification of overlap between CCL19 and GFAP IF signals in human gliosis and PCNSL brains compared with young control shown in (D).
(F) Two-month-old or 11-month-old WT mice were injected with E_μ-Myc LCs, and brains were harvested at terminal disease for analysis. n = 8 mice per group.
(G) Lesion sizes in brains from (F).
(H) B220 IHC of brains from mice in (F). Scale bars, 100 μm.
(I) Immunoblot analysis of GFAP and GAPDH protein in brain homogenates from 2-month-old compared with 11-month-old mice.
(J) Densitometric quantification of GFAP immunosignals shown in (I) normalized to GAPDH and expressed as percentage of 2-month-old (Ctrl).
(K) GFAP, Iba-1, CD68, Mac-3, and MHCII IHC of 2-month-old compared with 11-month-old brains. Scale bars, 100 μm (insets, 50 μm).
(L) Quantifications of immunoreactivity of IHC markers shown in (K) in 2-month-old compared with 11-month-old brains.
Black horizontal bars in (A), (B), (C), and (J) indicate the mean value. All error bars denote SEM. See also Figure S8. *$p < 0.05$, **$p < 0.01$, ***$p < 0.001$.

[Retrospective study of 48 cases of primary central nervous system lymphoma]. Medicina *77*, 17–23.

Ambady, P., Fu, R., Netto, J.P., Kersch, C., Firkins, J., Doolittle, N.D., and Neuwelt, E.A. (2017). Patterns of relapse in primary central nervous system lymphoma: inferences regarding the role of the neuro-vascular unit and monoclonal antibodies in treating occult CNS disease. Fluids Barriers CNS *14*, 16.

Bellan, C., Stefano, L., Giulia de, F., Rogena, E.A., and Lorenzo, L. (2009). Burkitt lymphoma versus diffuse large B-cell lymphoma: a practical approach. Hematol. Oncol. *27*, 182–185.

Bessell, E.M., Dickinson, P., Dickinson, S., and Salmon, J. (2011). Increasing age at diagnosis and worsening renal function in patients with primary central nervous system lymphoma. J. Neurooncol. *104*, 191–193.

Bhagavathi, S., Sharathkumar, A., Hunter, S., Sung, L., Kanhere, R., Venturina, M.D., and Wilson, J.D. (2008). Activated B-cell immunophenotype might be associated with poor prognosis of primary central nervous system lymphomas. Clin. Neuropathol. *27*, 13–20.

Bichi, R., Shinton, S.A., Martin, E.S., Koval, A., Calin, G.A., Cesari, R., Russo, G., Hardy, R.R., and Croce, C.M. (2002). Human chronic lymphocytic leukemia modeled in mouse by targeted TCL1 expression. Proc. Natl. Acad. Sci. U S A *99*, 6955–6960.

Birnbaum, T., Langer, S., Roeber, S., von Baumgarten, L., and Straube, A. (2013). Expression of B-cell activating factor, a proliferating inducing ligand and its receptors in primary central nervous system lymphoma. Neurol. Int. *5*, e4.

Bowman, E.P., Campbell, J.J., Soler, D., Dong, Z., Manlongat, N., Picarella, D., Hardy, R.R., and Butcher, E.C. (2000). Developmental switches in chemokine response profiles during B cell differentiation and maturation. J. Exp. Med. *191*, 1303–1318.

Brenner, M., Kisseberth, W.C., Su, Y., Besnard, F., and Messing, A. (1994). GFAP promoter directs astrocyte-specific expression in transgenic mice. J. Neurosci. *14*, 1030–1037.

Buonamici, S., Trimarchi, T., Ruocco, M.G., Reavie, L., Cathelin, S., Mar, B.G., Klinakis, A., Lukyanov, Y., Tseng, J.C., Sen, F., et al. (2009). CCR7 signalling as an essential regulator of CNS infiltration in T-cell leukaemia. Nature *459*, 1000–1004.

Camilleri-Broet, S., Criniere, E., Broet, P., Delwail, V., Mokhtari, K., Moreau, A., Kujas, M., Raphael, M., Iraqi, W., Sautes-Fridman, C., et al. (2006). A uniform activated B-cell-like immunophenotype might explain the poor prognosis of primary central nervous system lymphomas: analysis of 83 cases. Blood *107*, 190–196.

Chapuy, B., Stewart, C., Dunford, A.J., Kim, J., Kamburov, A., Redd, R.A., Lawrence, M.S., Roemer, M.G.M., Li, A.J., Ziepert, M., et al. (2018). Molecular subtypes of diffuse large B cell lymphoma are associated with distinct pathogenic mechanisms and outcomes. Nat. Med. *24*, 679–690.

Cheng, J., Tu, P., Shi, Q.L., Zhou, H.B., Zhou, Z.Y., Zhao, Y.C., Ma, H.H., and Zhou, X.J. (2008). [Primary diffuse large B-cell lymphoma of central nervous system belongs to activated B-cell-like subgroup: a study of 47 cases]. Zhonghua Bing Li Xue Za Zhi *37*, 384–389.

Choquet, S., Houillier, C., Bijou, F., Houot, R., Boyle, E., Gressin, R., Nicolas-Virelizier, E., Barrie, M., Molucon-Chabrot, C., Blonski, M., et al. (2016). Ibrutinib monotherapy in relapse or refractory primary CNS lymphoma (PCNSL) and primary vitreo-retinal lymphoma (PVRL). Result of the Interim analysis of the iLOC phase II study from the Lysa and the French LOC Network. Blood *128*, https://doi.org/10.1016/j.ejca.2019.05.024.

Columba-Cabezas, S., Serafini, B., Ambrosini, E., and Aloisi, F. (2003). Lymphoid chemokines CCL19 and CCL21 are expressed in the central nervous system during experimental autoimmune encephalomyelitis: implications for the maintenance of chronic neuroinflammation. Brain Pathol. *13*, 38–51.

Dave, S.S., Fu, K., Wright, G.W., Lam, L.T., Kluin, P., Boerma, E.J., Greiner, T.C., Weisenburger, D.D., Rosenwald, A., Ott, G., et al. (2006). Molecular diagnosis of Burkitt's lymphoma. N. Engl. J. Med. *354*, 2431–2442.

Deckert, M., Brunn, A., Montesinos-Rongen, M., Terreni, M.R., and Ponzoni, M. (2014a). Primary lymphoma of the central nervous system—a diagnostic challenge. Hematol. Oncol. *32*, 57–67.

Deckert, M., Montesinos-Rongen, M., Brunn, A., and Siebert, R. (2014b). Systems biology of primary CNS lymphoma: from genetic aberrations to modeling in mice. Acta Neuropathol. *127*, 175–188.

Engler, C., Kandzia, R., and Marillonnet, S. (2008). A one pot, one step, precision cloning method with high throughput capability. PLoS One *3*, e3647.

Ferreri, A.J., Cwynarski, K., Pulczynski, E., Ponzoni, M., Deckert, M., Politi, L.S., Torri, V., Fox, C.P., Rosee, P.L., Schorb, E., et al. (2016). Chemoimmunotherapy with methotrexate, cytarabine, thiotepa, and rituximab (MATRix regimen) in patients with primary CNS lymphoma: results of the first randomisation of the International Extranodal Lymphoma Study Group-32 (IELSG32) phase 2 trial. Lancet Haematol. *3*, e217–e227.

Fischer, L., Korfel, A., Pfeiffer, S., Kiewe, P., Volk, H.D., Cakiroglu, H., Widmann, T., and Thiel, E. (2009). CXCL13 and CXCL12 in central nervous system lymphoma patients. Clin. Cancer Res. *15*, 5968–5973.

Fritsch, K., Kasenda, B., Schorb, E., Hau, P., Bloehdorn, J., Mohle, R., Low, S., Binder, M., Atta, J., Keller, U., et al. (2017). High-dose methotrexate-based immuno-chemotherapy for elderly primary CNS lymphoma patients (PRIMAIN study). Leukemia *31*, 846–852.

Grommes, C., Pastore, A., Palaskas, N., Tang, S.S., Campos, C., Schartz, D., Codega, P., Nichol, D., Clark, O., Hsieh, W.Y., et al. (2017). Ibrutinib unmasks critical role of Bruton tyrosine kinase in primary CNS lymphoma. Cancer Discov. *7*, 1018–1029.

Harris, N.L., Stein, H., Coupland, S.E., Hummel, M., Favera, R.D., Pasqualucci, L., and Chan, W.C. (2001). New approaches to lymphoma diagnosis. Hematology Am. Soc. Hematol. Educ. Program, 194–220, https://doi.org/10.1182/asheducation-2001.1.194.

Hattab, E.M., Martin, S.E., Al-Khatib, S.M., Kupsky, W.J., Vance, G.H., Stohler, R.A., Czader, M., and Al-Abbadi, M.A. (2010). Most primary central nervous system diffuse large B-cell lymphomas occurring in immunocompetent individuals belong to the nongerminal center subtype: a retrospective analysis of 31 cases. Mod. Pathol. *23*, 235–243.

Heinig, K., Gatjen, M., Grau, M., Stache, V., Anagnostopoulos, I., Gerlach, K., Niesner, R.A., Cseresnyes, Z., Hauser, A.E., Lenz, P., et al. (2014). Access to follicular dendritic cells is a pivotal step in murine chronic lymphocytic leukemia B-cell activation and proliferation. Cancer Discov. *4*, 1448–1465.

Henning, G., Ohl, L., Junt, T., Reiterer, P., Brinkmann, V., Nakano, H., Hohenberger, W., Lipp, M., and Forster, R. (2001). CC chemokine receptor 7-dependent and -independent pathways for lymphocyte homing: modulation by FTY720. J. Exp. Med. *194*, 1875–1881.

Herrmann, O., Baumann, B., de Lorenzi, R., Muhammad, S., Zhang, W., Kleesiek, J., Malfertheiner, M., Kohrmann, M., Potrovita, I., Maegele, I., et al. (2005). IKK mediates ischemia-induced neuronal death. Nat. Med. *11*, 1322–1329.

Hochberg, F.H., Baehring, J.M., and Hochberg, E.P. (2007). Primary CNS lymphoma. Nat. Clin. Pract. Neurol. *3*, 24–35.

Horvat, M., Zadnik, V., Juznic Setina, T., Boltezar, L., Pahole Golicnik, J., Novakovic, S., and Jezersek Novakovic, B. (2018). Diffuse large B-cell lymphoma: 10 years' real-world clinical experience with rituximab plus cyclophosphamide, doxorubicin, vincristine and prednisolone. Oncol. Lett. *15*, 3602–3609.

Housley, W.J., Pitt, D., and Hafler, D.A. (2015). Biomarkers in multiple sclerosis. Clin. Immunol. *161* (1), 51–58.

Hoyer, K.K., French, S.W., Turner, D.E., Nguyen, M.T., Renard, M., Malone, C.S., Knoetig, S., Qi, C.F., Su, T.T., Cheroutre, H., et al. (2002). Dysregulated TCL1 promotes multiple classes of mature B cell lymphoma. Proc Natl Acad Sci U S A *99*, 14392–14397.

Husseini, L., Saleh, A., Reifenberger, G., Hartung, H.P., and Kieseier, B.C. (2012). Inflammatory demyelinating brain lesions heralding primary CNS lymphoma. Can. J. Neurol. Sci. *39*, 6–10.

Kienast, Y., von Baumgarten, L., Fuhrmann, M., Klinkert, W.E., Goldbrunner, R., Herms, J., and Winkler, F. (2010). Real-time imaging reveals the single steps of brain metastasis formation. Nat. Med. *16*, 116–122.

Krumbholz, M., Theil, D., Derfuss, T., Rosenwald, A., Schrader, F., Monoranu, C.M., Kalled, S.L., Hess, D.M., Serafini, B., Aloisi, F., et al. (2005). BAFF is

produced by astrocytes and up-regulated in multiple sclerosis lesions and primary central nervous system lymphoma. J. Exp. Med. *201*, 195–200.

Krumbholz, M., Theil, D., Steinmeyer, F., Cepok, S., Hemmer, B., Hofbauer, M., Farina, C., Derfuss, T., Junker, A., Arzberger, T., et al. (2007). CCL19 is constitutively expressed in the CNS, up-regulated in neuroinflammation, active and also inactive multiple sclerosis lesions. J. Neuroimmunol. *190*, 72–79.

Labun, K., Montague, T.G., Gagnon, J.A., Thyme, S.B., and Valen, E. (2016). CHOPCHOP v2: a web tool for the next generation of CRISPR genome engineering. Nucleic Acids Res. *44*, W272–W276.

Lattke, M., Magnutzki, A., Walther, P., Wirth, T., and Baumann, B. (2012). Nuclear factor kappaB activation impairs ependymal ciliogenesis and links neuroinflammation to hydrocephalus formation. J. Neurosci. *32*, 11511–11523.

Lee, J.H., Jeong, H., Choi, J.W., Oh, H., and Kim, Y.S. (2017). Clinicopathologic significance of MYD88 L265P mutation in diffuse large B-cell lymphoma: a meta-analysis. Sci. Rep. *7*, 1785.

Lionakis, M.S., Dunleavy, K., Roschewski, M., Widemann, B.C., Butman, J.A., Schmitz, R., Yang, Y., Cole, D.E., Melani, C., Higham, C.S., et al. (2017). Inhibition of B cell receptor signaling by ibrutinib in primary CNS lymphoma. Cancer Cell *31*, 833–843.e5.

Lu, J.Q., O'Kelly, C., Girgis, S., Emery, D., Power, C., and Blevins, G. (2016). Neuroinflammation preceding and accompanying primary central nervous system lymphoma: case study and literature review. World Neurosurg. *88*, 692.e1-8.

Lynch, A.M., Murphy, K.J., Deighan, B.F., O'Reilly, J.A., Gun'ko, Y.K., Cowley, T.R., Gonzalez-Reyes, R.E., and Lynch, M.A. (2010). The impact of glial activation in the aging brain. Aging Dis. *1*, 262–278.

Lyons, M.K., Boucher, O.K., Birch, B.D., and Patel, N.P. (2011). The development of primary central nervous system B-cell lymphoma in multiple sclerosis. Neurohospitalist *1*, 133–136.

Mahadevan, A., Rao, C.R., Shanmugham, M., and Shankar, S.K. (2015). Primary central nervous system diffuse large B-cell lymphoma in the immunocompetent: Immunophenotypic subtypes and Epstein-Barr virus association. J. Neurosci. Rural Pract. *6*, 8–14.

McCandless, E.E., Wang, Q., Woerner, B.M., Harper, J.M., and Klein, R.S. (2006). CXCL12 limits inflammation by localizing mononuclear infiltrates to the perivascular space during experimental autoimmune encephalomyelitis. J. Immunol. *177*, 8053–8064.

Mercurio, F., Zhu, H., Murray, B.W., Shevchenko, A., Bennett, B.L., Li, J., Young, D.B., Barbosa, M., Mann, M., Manning, A., et al. (1997). IKK-1 and IKK-2: cytokine-activated IkappaB kinases essential for NF-kappaB activation. Science *278*, 860–866.

Montague, T.G., Cruz, J.M., Gagnon, J.A., Church, G.M., and Valen, E. (2014). CHOPCHOP: a CRISPR/Cas9 and TALEN web tool for genome editing. Nucleic Acids Res. *42*, W401–W407.

Montesinos-Rongen, M., Godlewska, E., Brunn, A., Wiestler, O.D., Siebert, R., and Deckert, M. (2011). Activating L265P mutations of the MYD88 gene are common in primary central nervous system lymphoma. Acta Neuropathol. *122*, 791–792.

Montesinos-Rongen, M., Purschke, F.G., Brunn, A., May, C., Nordhoff, E., Marcus, K., and Deckert, M. (2015). Primary central nervous system (CNS) lymphoma B cell receptors recognize CNS proteins. J. Immunol. *195*, 1312–1319.

Nagle, S.J., Shah, N.N., Ganetsky, A., Landsburg, D.J., Nasta, S.D., Mato, A., Schuster, S.J., Reshef, R., Tsai, D.E., and Svoboda, J. (2017). Long-term outcomes of rituximab, temozolomide and high-dose methotrexate without consolidation therapy for lymphoma involving the CNS. Int. J. Hematol. Oncol. *6*, 113–121.

Nasr, M.R., Rosenthal, N., and Syrbu, S. (2010). Expression profiling of transcription factors in B- or T-acute lymphoblastic leukemia/lymphoma and burkitt lymphoma: usefulness of PAX5 immunostaining as pan-Pre-B-cell marker. Am. J. Clin. Pathol. *133*, 41–48.

Nawijn, M.C., Alendar, A., and Berns, A. (2011). For better or for worse: the role of Pim oncogenes in tumorigenesis. Nat. Rev. Cancer *11*, 23–34.

Nayak, L., Iwamoto, F.M., LaCasce, A., Mukundan, S., Roemer, M.G.M., Chapuy, B., Armand, P., Rodig, S.J., and Shipp, M.A. (2017). PD-1 blockade with nivolumab in relapsed/refractory primary central nervous system and testicular lymphoma. Blood *129*, 3071–3073.

Oeckl, P., Lattke, M., Wirth, T., Baumann, B., and Ferger, B. (2012). Astrocyte-specific IKK2 activation in mice is sufficient to induce neuroinflammation but does not increase susceptibility to MPTP. Neurobiol. Dis. *48*, 481–487.

Pascual, O., Casper, K.B., Kubera, C., Zhang, J., Revilla-Sanchez, R., Sul, J.Y., Takano, H., Moss, S.J., McCarthy, K., and Haydon, P.G. (2005). Astrocytic purinergic signaling coordinates synaptic networks. Science *310*, 113–116.

Phelan, J.D., Young, R.M., Webster, D.E., Roulland, S., Wright, G.W., Kasbekar, M., Shaffer, A.L., 3rd, Ceribelli, M., Wang, J.Q., Schmitz, R., et al. (2018). A multiprotein supercomplex controlling oncogenic signalling in lymphoma. Nature *560*, 387–391.

Rehm, A., Mensen, A., Schradi, K., Gerlach, K., Wittstock, S., Winter, S., Buchner, G., Dorken, B., Lipp, M., and Hopken, U.E. (2011). Cooperative function of CCR7 and lymphotoxin in the formation of a lymphoma-permissive niche within murine secondary lymphoid organs. Blood *118*, 1020–1033.

Reif, K., Ekland, E.H., Ohl, L., Nakano, H., Lipp, M., Forster, R., and Cyster, J.G. (2002). Balanced responsiveness to chemoattractants from adjacent zones determines B-cell position. Nature *416*, 94–99.

Rubenstein, J.L., Wong, V.S., Kadoch, C., Gao, H.X., Barajas, R., Chen, L., Josephson, S.A., Scott, B., Douglas, V., Maiti, M., et al. (2013). CXCL13 plus interleukin 10 is highly specific for the diagnosis of CNS lymphoma. Blood *121*, 4740–4748.

Ruddle, N.H. (2014). Lymphotoxin and TNF: how it all began-a tribute to the travelers. Cytokine Growth Factor Rev. *25*, 83–89.

Sanjana, N.E., Shalem, O., and Zhang, F. (2014). Improved vectors and genome-wide libraries for CRISPR screening. Nat. Methods *11*, 783–784.

Schindelin, J., Arganda-Carreras, I., Frise, E., Kaynig, V., Longair, M., Pietzsch, T., Preibisch, S., Rueden, C., Saalfeld, S., Schmid, B., et al. (2012). Fiji: an open-source platform for biological-image analysis. Nat. Methods *9*, 676–682.

Schlager, C., Korner, H., Krueger, M., Vidoli, S., Haberl, M., Mielke, D., Brylla, E., Issekutz, T., Cabanas, C., Nelson, P.J., et al. (2016). Effector T-cell trafficking between the leptomeninges and the cerebrospinal fluid. Nature *530*, 349–353.

Schneider, C.A., Rasband, W.S., and Eliceiri, K.W. (2012). NIH Image to ImageJ: 25 years of image analysis. Nat. Methods *9*, 671–675.

Sierra del Rio, M., Rousseau, A., Soussain, C., Ricard, D., and Hoang-Xuan, K. (2009). Primary CNS lymphoma in immunocompetent patients. Oncologist *14*, 526–539.

Smedby, K.E., Baecklund, E., and Askling, J. (2006a). Malignant lymphomas in autoimmunity and inflammation: a review of risks, risk factors, and lymphoma characteristics. Cancer Epidemiol. Biomarkers Prev. *15*, 2069–2077.

Smedby, K.E., Hjalgrim, H., Askling, J., Chang, E.T., Gregersen, H., Porwit-MacDonald, A., Sundstrom, C., Akerman, M., Melbye, M., Glimelius, B., et al. (2006b). Autoimmune and chronic inflammatory disorders and risk of non-Hodgkin lymphoma by subtype. J. Natl. Cancer Inst. *98*, 51–60.

Thaler, F.S., Laurent, S.A., Huber, M., Mulazzani, M., Dreyling, M., Kodel, U., Kumpfel, T., Straube, A., Meinl, E., and von Baumgarten, L. (2017). Soluble TACI and soluble BCMA as biomarkers in primary central nervous system lymphoma. Neuro. Oncol. *19*, 1618–1627.

Tigges, U., Komatsu, M., and Stallcup, W.B. (2013). Adventitial pericyte progenitor/mesenchymal stem cells participate in the restenotic response to arterial injury. J. Vasc. Res. *50*, 134–144.

Tomita, N., Yokoyama, M., Yamamoto, W., Watanabe, R., Shimazu, Y., Masaki, Y., Tsunoda, S., Hashimoto, C., Murayama, K., Yano, T., et al. (2018). The standard international prognostic index for predicting the risk of CNS involvement in DLBCL without specific prophylaxis. Leuk. Lymphoma *59*, 97–104.

Tun, H.W., Personett, D., Baskerville, K.A., Menke, D.M., Jaeckle, K.A., Kreinest, P., Edenfield, B., Zubair, A.C., O'Neill, B.P., Lai, W.R., et al. (2008). Pathway analysis of primary central nervous system lymphoma. Blood *111*, 3200–3210.

Villano, J.L., Koshy, M., Shaikh, H., Dolecek, T.A., and McCarthy, B.J. (2011). Age, gender, and racial differences in incidence and survival in primary CNS lymphoma. Br. J. Cancer *105*, 1414–1418.

von Baumgarten, L., Brucker, D., Tirniceru, A., Kienast, Y., Grau, S., Burgold, S., Herms, J., and Winkler, F. (2011). Bevacizumab has differential and dose-dependent effects on glioma blood vessels and tumor cells. Clin. Cancer Res. *17*, 6192–6205.

Wang, C.W., Ka, S.M., and Chen, A. (2014). Robust image registration of biological microscopic images. Sci. Rep. *4*, 6050.

Williams, R.L., Risau, W., Zerwes, H.G., Drexler, H., Aguzzi, A., and Wagner, E.F. (1989). Endothelioma cells expressing the polyoma middle T oncogene induce hemangiomas by host cell recruitment. Cell *57*, 1053–1063.

Wilson, W.H., Young, R.M., Schmitz, R., Yang, Y., Pittaluga, S., Wright, G., Lih, C.J., Williams, P.M., Shaffer, A.L., Gerecitano, J., et al. (2015). Targeting B cell receptor signaling with ibrutinib in diffuse large B cell lymphoma. Nat. Med. *21*, 922–926.

Wong, S., and Fulcher, D. (2004). Chemokine receptor expression in B-cell lymphoproliferative disorders. Leuk. Lymphoma *45*, 2491–2496.

STAR★METHODS

KEY RESOURCES TABLE

REAGENT or RESOURCE	SOURCE	IDENTIFIER
Antibodies		
Murine F4/80	BMA Biomedicals AG	Cat# T-2006; RRID: AB_1227368
Murine B220	BD Biosciences	Cat# 553084; RRID: AB_394614
Murine c-myc	Abcam	Cat# ab32072; RRID: AB_731658
Murine Ki67	NeoMarkers	Cat# RM-9106-S0; RRID: AB_2341197
Murine MHCII	Novus Biologicals	Cat# NBP1-43312; RRID: AB_10006679
Murine CD4	eBioscience	Cat# 14-9766; RRID: AB_2573007
Murine IRF4	Acris	Cat# AP01237PU-N; RRID: AB_1618519
Murine Bcl2	Aviva Systems Biology	Cat# OAPB00242
Murine CD31	Abcam	Cat# ab28364; RRID: AB_726362
Murine Iba-1	Abcam	Cat# ab178846; RRID: AB_2636859
Murine CXCL12	R&D Systems	Cat# MAB350; RRID: AB_2088149
FITC-CD49d	Biolegend	Cat# 103606; RRID: AB_313037
FITC-Rat IgG2b Isotype	Biolegend	Cat# 400606; RRID: AB_326550
Alexa Fluor 488-CCR7	Biolegend	Cat# 120112; RRID: AB_492842
Alexa Fluor 488-Rat IgG2a Isotype	Biolegend	Cat# 400525
FITC-CD11a	Biolegend	Cat# 101006; RRID: AB_312711
FITC-CXCR5	BD Biosciences	Cat# 561989; RRID: AB_10896978
APC-CXCR4	eBioscience	Cat# 17-9991-82; RRID: AB_10670878
APC-Rat IgG2b Isotype	eBioscience	Cat# 17-4031-82; RRID: AB_470176
PE/Dazzle-B220	Biolegend	Cat# 103258; RRID: AB_2564053
BV421-CD11c	Biolegend	Cat# 117329; RRID; AB_10897814
BV421-CD11b	Biolegend	Cat# 101235; RRID: AB_10897942
PE-CD3	Biolegend	Cat# 100205; RRID: AB_312662
Alexa Fluor 700-CD45	Biolegend	Cat# 103127; RRID: AB_493714
LTα	Genentech	Cat# Clone s5H3.2.2
LTα	R&D Systems	Cat# BAF749; RRID: AB_2138744
Murine CCL19	R&D Systems	Cat# AF880; RRID: AB_2071545
Murine EEA1	Abcam	Cat# ab2900; RRID: AB_2262056
Murine GFAP	Abcam	Cat# ab4674; RRID: AB_304558
Murine IgM	BD Biosciences	Cat# 553405; RRID: AB_394842
Murine CD11b	BMA Biomedicals AG	Cat# T-2102; RRID: AB_1227253
Murine / Human GFAP	Sigma-Aldrich	Cat# G6171; RRID: AB_1840893
Murine N-Cadherin	Cell Signaling	Cat# 4061; RRID: AB_10694647
GAPDH	Cell Signaling	Cat# 2118; RRID: AB_561053
Murine PSD-95	R&D Systems	Cat# PPS059; RRID: AB_2261668
Biotinylated CD45.2	eBioscience	Cat# 13-0454-82; RRID: AB_466456
Murine CXCL12	R&D Systems	Cat# BAF310; RRID: AB_356384
Biotinylated CD11c	eBioscience	Cat# 13-0114; RRID: AB_466363
Biotinylated CD31	eBioscience	Cat# 13-0311; RRID: AB_466419
Human PE-Tcl1	Biolegend	Cat# 330506; RRID: AB_2204407
Human CCL19	R&D Systems	Cat# AF361; RRID: AB_355323
Human CD20	Abcam	Cat# ab9475; RRID: AB_307267
Human CCR7	Sigma-Aldrich	Cat# SAB4500329; RRID: AB_10761024

(*Continued on next page*)

Continued

REAGENT or RESOURCE	SOURCE	IDENTIFIER
Biological Samples		
Human PCNSL, SCNSL, and healthy brain samples	Institute of Neuropathology, University of Freiburg, DE	N/A
Human PCNSL and healthy control CSF	Department of Hematology, Oncology, and Stem Cell Transplantation, University of Freiburg, DE	N/A
Human PCNSL, SCNSL, and control CSF	Department of Neurology, Ludwig-Maximilians University, Munich, DE	Thaler et al., 2017
Healthy human brain mRNA	Thermofisher	Cat# AM7962
Chemicals, Peptides, and Recombinant Proteins		
ACH6	Biogen	N/A
papain	Sigma-Aldrich	Cat# P4762
DNase I	Sigma-Aldrich	Cat# D5025
Recombinant mouse CCL19	R&D Systems	Cat# 440-M3-025
lipofectamine	Thermofisher	Cat# 116680
Dynabeads Biotin Binder	Thermofisher	Cat# 11047
Recombinant mouse TNFα	Thermofisher	RMTNFAI
Recombinant mouse CXCL12	R&D Systems	Cat# 460-SD
AMD3100	Sigma-Aldrich	Cat# A5602
luciferin	PJK GmbH	N/A
CMTPX	Thermofisher	Cat# C34552
Critical Commercial Assays		
Mouse CCL19 ELISA	R&D Systems	Cat# DY440
Human CCL19 ELISA	R&D Systems	Cat# DY361
Mouse XL Cytokine Array	R&D Systems	Cat# ARY028
RNeasy Lipid Mini Kit	Qiagen	Cat# 74804
RNeasy Mini Kit	Qiagen	Cat# 74104
Quantitect Reverse Transcriptase Kit	Qiagen	Cat# 205310
Deposited Data		
Mass spectrometry proteomics data	Proteome Xchange Consortium	Cat# PXD014099
Experimental Models: Cell Lines		
E_μ-myc "665" B-cell lymphoma cell line	Laboratory of Ulrich Keller; Charité, Berlin	N/A
sEnd.1 mouse endothelial cell line	Williams et al., 1989	RRID: CVCL_6270
HEK293T	ATCC	CRL-3216; RRID: CVCL_0063
Experimental Models: Organisms/Strains		
C57BL/6J mice	Charles River Laboratories; Sulzfeld, Germany	RRID: IMSR_JAX000664
GFAP-LTαβ mice	This paper	N/A
GFAP-tTA-IKK2CA mice	Lattke et al., 2012; Oeckl et al., 2012	N/A
Paucity of lymph node T-cells "plt" mice	Henning et al., 2001	N/A
Aged C57BL/6 mice	Janvier Labs; Le Genest-Saint-Isle, France	N/A
E_μ-myc mice	Adams et al., 1985	N/A
E_μ-Tcl1 mice	Bichi et al., 2002	N/A
Oligonucleotides		
Murine qPCR primers; See Table S2	This paper	N/A
Human qPCR primer sequences; See Table S3	This paper	N/A

(*Continued on next page*)

Continued		
REAGENT or RESOURCE	SOURCE	IDENTIFIER
Murine CXCR4 single guide RNA sequence: ATC TTT GCC GAC GTC AGC CA	This paper	N/A
Murine CCR7 single guide 1 RNA sequence: TGAAGCACACCGACTCGTAC	This paper	N/A
Murine CCR7 single guide 2 RNA sequence: CTACATCGGCGAGAATACCA	This paper	N/A
Murine CCR7 single guide 3 RNA sequence: CATCGGCGAGAATACCACGG	This paper	N/A
GFAP-LTαβ transgene genotyping primer "GFAP-fwd 3": CAGAGCAGGTTGGAGAGG	This paper	N/A
GFAP-LTαβ transgene genotyping primer "LTα rev": CAGAGAAAACCACCTGGGAG	This paper	N/A
GFAP-LTαβ transgene genotyping primer "LTβ rev": GAGTCTCTGAGAGGCTAGAG	This paper	N/A
GFAP-LTαβ cloning primer "LTa fw BamHI": cggggatcccagactatcatcatgacactgctcggccgtctcc		
GFAP-LTαβ cloning primer "LTa rev BamHI": cggggatccaatctacagtgcaaaggctcc		
GFAP-LTαβ cloning primer "LTb fw BamHI": cggggatcccagactatcatcatcgggacacggggactgcaggg		
GFAP-LTαβ cloning primer "LTb rev BamHI": cggggatccaattcaccccaccatcaccgc		
Recombinant DNA		
lentiCRISPR v2	Sanjana et al., 2014	RRID: Addgene_52961
pGfa2-nLac	Brenner et al., 1994	RRID: Addgene_53126
Software and Algorithms		
ImageJ	Schneider et al., 2012	RRID: SCR_003070
CwR plugin for ImageJ	Wang et al., 2014	N/A
Imaris	Oxford Instruments	RRID: SCR_007370
iMovie	Apple	N/A
GraphPad	Prism	RRID: SCR_002798

LEAD CONTACT AND MATERIALS AVAILABILITY

Further information and requests for resources and reagents should be directed to and will be fulfilled by the Lead Contact, Mathias Heikenwälder (m.heikenwaelder@dkfz-heidelberg.de)

EXPERIMENTAL MODEL AND SUBJECT DETAILS

All animal procedures were carried out in strict accordance with EU animal laws and were approved by the government of Bavaria (animal license no. 55.2-1-55-2532-178-15; 55.2-1-55-2532-196-13). Human specimens were acquired with written informed consent, with the approval of the local ethics committee of the University of Freiburg, and according to the local ethics guidelines in Munich and the Declaration of Helsinki.

GFAP-LTαβ Mice

For creation of GFAP-LTαβ transgenic mice, the *LacZ* sequence was excised from pGfa2-nLac (Brenner et al., 1994) using *BamHI*. Murine lymphotoxin α (*LTA*; NM_010735.2) cDNA was amplified with the primers LTa fw BamHI: 5' – cggggatcccagactatcatcatga cactgctcggccgtctcc – 3' and LTa rev BamHI: 5' – cggggatccaatctacagtgcaaaggctcc – 3'. Murine lymphotoxin β cDNA (*LTB*; NM_008518.2) was amplified with the primers LTb fw BamHI: 5' - cggggatcccagactatcatcatcgggacacggggactgcaggg - 3' and LTb rev BamHI: 5' - cggggatccaattcaccccaccatcaccgc - 3'. *LTA* and *LTB* amplicons were digested with BamHI, purified, and ligated into pGfa2 backbone. GFAP-LTα and GFAP-LTβ transgenes were used for pro-nuclear co-injection into pseudo-pregnant C57BL/6J females, resulting in three founder lines: #8, #23, and #26. The line #26 was used for the current study. Animals were maintained as single transgenics on a C57BL/6J background under SPF conditions. Transgene-positive animals were identified *via* PCR with

the primers GFAP-fwd 3 – 5' -cagagcaggttggagagg -3', LTα rev: 5' -cagagaaaaccacctgggag - 3', and LTβ rev: 5' – gagtctctgagaggc tagag – 3'. Both male and female animals were used for experiments after two months of age. Non-transgenic littermates were used as controls.

GFAP-tTA-IKK2CA Mice

GFAP-tTA-IKK2CA ("IKK2CA") mice (Lattke et al., 2012; Oeckl et al., 2012) co-express a transgene encoding tetracycline-inducible, constitutively active IKK2 kinase containing S177E and S181E point mutations in the IKK2 kinase domain [$(tetO)_7$-IKK2CA] (Herrmann et al., 2005; Mercurio et al., 1997) and the tetracycline transactivating domain under the control of the GFAP promoter (GFAP-tTA) (Pascual et al., 2005). IKK2CA expression was repressed by exposure to 0.5 g/L doxycycline (MP Biochemicals) in 1% sucrose in the drinking water embryonically and up to 4 weeks postnatally. Mice were maintained on a C57BL/6J background under SPF conditions. Both males and females were used for experiments after two months of age. Non-transgenic and single transgenic littermates were used as controls.

Plt Mice

Paucity of lymph node T cell "Plt" mice on a C57BL/6 background lacking endogenous CCL19 and CCL21 (Henning et al., 2001) were kindly provided by Reinhold Förster and bred to the GFAP-LTαβ line in-house to produce plt/plt × GFAP-LTα$\beta^{Tg/WT}$ mice. Mice were administered 1 × 10^6 E_μ-Myc lymphoma cells i.v. and allowed to progress to terminal illness. Both males and females were used for experiments after two months of age.

Aged Mice

For aged mouse experiments, 12 two-month old (young) and eleven-month old (old) C57BL/6 mice were purchased from Janvier Labs. Four young and four old uninjected animals were sacrificed for biochemical and histological analyses. The remaining mice were injected with 1 × 10^6 "primary" E_μ-Myc lymphoma cells, and brains were collected for analysis at terminal disease.

"Primary" E_μ-Myc Lymphoma Cells

Primary E_μ-Myc lymphoma cells were isolated from lymph nodes of terminally ill "E_μ-Myc" transgenic mice, which express a rearranged version of the *CMYC* oncogene cloned from the murine ABPC17 plasmocytoma cell line under the control of the μ immunoglobulin Ig_H locus enhancer (Adams et al., 1985). E_μ-Myc mice are on a C57BL/6 background. To induce terminal disease in C57BL/6 mice with 100% incidence, 1 × 10^6 E_μ-Myc lymphoma cells were administered i.v., and terminal illness generally ensued within 4 weeks, marked by weight loss, lethargic behavior, and swollen lymph nodes.

"Primary" E_μ-Tcl1 Lymphoma Cells

E_μ-Tcl1 mice were created by pro-nuclear injection of the human *TCL1* coding region expressed under the control of the mouse V_H promoter and $Ig_{H\text{-}\mu}$ enhancer (Bichi et al., 2002). E_μ-Tcl1 mice were originally created on a B6C3 background and were subsequently crossed for more than ten generations on a pure C57BL/6 background (Heinig et al., 2014). Splenocytes isolated from terminally ill founder line "F10" mice were used for the current study. For primary lymphoma cell suspensions, spleens were isolated from terminal E_μ-Tcl1 animals, passed through a 70 μm cell strainer with 1x PBS, re-suspended in 10% DMSO in fetal bovine serum (FBS), frozen at -80°C, and transferred to liquid nitrogen for long-term storage. For tumor cell administration, 1 × 10^6 E_μ-Tcl1 lymphoma cells were re-suspended in 50 μL sterile 1x PBS and injected intravenously.

Ccr7$^{-/-}$ E_μ-Myc Cells

Ccr7$^{-/-}$ E_μ-Myc cells were isolated from lymph nodes of *Ccr7*$^{-/-}$ E_μ-$Myc^{Tg/+}$ animals on a C57BL/6 background (Rehm et al., 2011). "Primary" E_μ-Myc cells harvested from lymph nodes of E_μ-Myc transgenic mice (and WT at the *Ccr7* locus) were used as control lymphoma cells for the *Ccr7*$^{-/-}$ and experiments.

Primary Glia Cultures

To obtain primary glial cultures, brains were isolated from postnatal day 0 (P0) pups derived from a GFAP-LTα$\beta^{Tg/WT}$ x GFAP-LTα$\beta^{WT/WT}$ or WT C57BL/6 breeding, dissociated with 0.25% trypsin for 15 minutes at 37°C, washed 3x for 5 min. with complete DMEM, triturated with a P1000 pipette, and plated in a 24-well plate (4 wells/ brain) in DMEM containing 10% Hyclone FBS and 1% pen-strep. Media was replaced every 48 hr, and glia were allowed to grow to confluency (at least two weeks after plating) before being used for experiments. Tissue from each P0 pup was used for PCR and assignment of GFAP-LTαβ positivity or negativity for each culture (see "GFAP-LTαβ mice" above for transgene-specific primer sequences).

E_μ-Myc "665" Lymphoma Cell Line

The B cell lymphoma cell line "665" was created by isolation of lymphoma cells from lymph nodes of terminally ill E_μ-Myc transgenic mice. Isolated lymphoma cells were cultured in the presence of 6.25 ng/mL interleukin-7 (IL-7; Cat. # 407-ML-005; R&D Systems) and a stromal cell line which were gradually reduced over a period of 2 – 3 months. 665 cells were maintained in 10% Hyclone FBS, 1% pen-strep, and 1% non-essential amino acids (NEAA) in RPMI supplemented with 50 μM β-mercaptoethanol. 665 cells were split 1:10 daily. For freezing, 10 × 10^6 665 cells were frozen in 1 mL of complete medium containing 10% DMSO. In the first passage

after thawing, 665 cells were supplemented with 6.25 ng/mL IL-7. To induce terminal disease in C57BL/6 mice, 2×10^4 665 cells were injected i.v., and mice reached terminal disease by 4 weeks post-injection. For 24 hr. experiments, mice were injected with 1×10^6 665 cells i.v., and mice were sacrificed 24 hr post-injection.

sEnd.1 Cell Line

The murine endothelial cell line, sEnd.1; (Williams et al., 1989) was maintained in 10% Hyclone FBS and 1% pen-strep in DMEM.

Human Samples

Twelve surgical brain biopsies from six male and six female human brains with a median age of 74 diagnosed with primary CNS lymphoma, 5 male and 2 female patients with a median age of 61 diagnosed with peripheral lymphoma with CNS involvement (SCNSL), and 6 male and 4 female patients with median age of 53 diagnosed with non-specific gliosis from the Department of Neuropathology in Freiburg, Germany were used for mRNA expression analysis and compared to cDNA copied from three to six separate aliquots of age-matched normal human brain mRNA purchased from Thermofisher (AM7962). For IF analysis, cryopreserved brain biopsies from six PCNSL cases with a median age of 78, as well as three surgical biopsies from patients with a median age of 32 diagnosed with non-specific gliosis, 3 males and 1 female young human control brains with median age of 17 from the Department of Neuropathology in Freiburg, Germany, and normal human lymph node were used. Healthy human CSF donors ranged from ages 18 to 83 with a median age of 36.5, PCNSL CSF donors ranged from ages 37 to 84 with a median age of 70, and SCNSL donors ranged in age from 53 to 71 with a median age of 65.5. CSF samples were provided by the Department of Neurology at Ludwigs-Maximillians University and the Department of Hematology, Oncology, and Stem Cell Transplantation in Freiburg, Germany.

METHOD DETAILS

Animals and Treatments

For tumor cell administration, 2×10^4 "665" E_μ-Myc cells or 1×10^6 "primary" E_μ-Myc or E_μ-Tcl1 lymphoma cells were re-suspended in 50 μL sterile 1x PBS and injected intravenously. For LTβR agonist experiments, C57BL/6 mice were administered 50 μg ACH6 (Biogen Idec) intraperitoneally starting 2 months after administration of 1×10^6 E_μ-Tcl1 lymphoma cells. Animals were then boostered weekly with 50 μg ACH6 until terminal disease. For short-term experiments, animals were injected with 1×10^6 E_μ-Myc, or *Cxcr4*$^{-/-}$ E_μ-Myc lymphoma cells i.v. and euthanized 24 hr later for analysis. For short-term experiments with ACH6, animals were injected i.p. with 50 μg ACH6 24 hr prior to lymphoma cell administration and then boostered with an additional 50 μg ACH6 i.p. just before lymphoma cell administration. Animals were euthanized via carbon dioxide inhalation, and organs were harvested for analysis.

Brain Cell Isolation

The isolation procedure was adapted from (Tigges et al., 2013). Brains from GFAP-LTαβ mice or NTg littermates were isolated and minced with a razor blade. Brains were re-suspended in 5 mL complete DMEM containing 30 U/mL papain and 200 U/mL DnaseI and incubated at 37°C for 70 min. Brain homogenates were passed 10x through an 18G needle and then 10x through a 21G needle. The brain homogenates were diluted in 1.7 volumes of 22% BSA in 1x PBS and then centrifuged at 4,000 r.p.m. at 4°C for 10 min. Cells were re-suspended in 1mL of complete DMEM containing 10 μg biotinylated anti-CD45.2 or anti-CD31 and incubated at 4°C for 10 min. Cells were washed with 2 mL complete DMEM and centrifuged at 350 x g for 5 min. Cells were re-suspended and incubated with magnetic biotin-binding Dynabeads for 30 min. at 4°C. Bound cells were washed, collected with a magnet, and isolated in RLT buffer (Qiagen) for mRNA analysis.

Mass Spectrometry-Based Proteomics analysis

Brain homogenates were reduced using DTT at final concentration of 10 mM, sonicated, and cooled to room temperature. Proteins were alkylated using 55 mM iodoacetamide. Proteins were precipitated using cold 80% acetone overnight. Protein precipitates were washed with 80% acetone and pelleted by centrifugation. The dried pellet was then resuspended in 50 μL of 2M thiourea/6M urea in 10 mM HEPES at pH 8.0. Digestion of protein into peptides was performed using a 4 hour predigestion with LysC (1:100 ratio). The pre-digest was diluted 1:4 using 50 mM ammonium bicarbonate (pH 8.0), and overnight digestion was performed using 1:100 trypsin. Desalting of digested peptides was performed using a C18-based solid-phase extraction. Peptides corresponding to a volume of 10 μg of protein were added and bound to the stage tips. The bound peptides were washed with 0.1% formic acid and eluted from the solid support using 40 μL of 80% acetonitrile with 0.1% formic acid, and subsequently lyophilized. Dried peptides were re-suspended in 0.1% formic acid and peptide concentration was measured using a Nanodrop. For each sample, 0.5 μg of peptides were used for MS-based proteomic analysis. Additionally, a pool of peptides was prepared by mixing 2 μg of peptides from each sample, and subsequently fractioned into 8-fractions using high-pH reverse phase chromatography. Each sample and the pooled sample were analyzed using a 2 hr. C18-based reverse phase chromatography. Peptides were separated using an EASY-nLC 1200 HPLC system (Thermo Fisher Scientific) coupled online to the QExactive HFX tandem mass spectrometer via a nanoelectrospray source (Thermo Fisher Scientific). Peptides were eluted using a 120 min. gradient of 5–60% buffer B (80% acetonitrile and 0.5% formic acid) at a flow rate of 300 nl/min and a column temperature of 55°C. Data was obtained in a data-dependent Top15 acquisition mode. All MS1 scans were acquired at resolution of 60,000 with AGC target of 3e6, whereas MS2 scans were acquired at a resolution of 15,000 with AGC target of 1e5. The acquired raw data was analyzed using MaxQuant (1.6.2.10) using mouse uniprot isoform

(version: 2019-02-21, number of sequences: 25233) and TrEMBL (version:2019-02-21, number of sequences: 68150) protein sequence fastas. FDR was set to 1% on peptide protein level to control for false-positive identification of peptides. All proteins detected with at least two peptides were carried forward in the analysis. Enrichment analysis was performed using 1D Enrichment for differential enrichment in NTg vs GFAP-LTαβ brains, and ClusterProfiler for over-representation analysis of Wikipathways and MSigDB in the acquired data. From significantly enriched terms, proteins with 1.2x higher intensity in the test samples and the top 20 proteins with the largest variance are visualized as heat maps. In the heat maps, proteins are placed in accordance to their Pearson correlations and are furthered divided into unsupervised clusters using K-means.

Cell Culture

For proliferation assays, NTg or GFAP-LTαβ primary glia media was conditioned for 24 hr and then transferred to a fresh tissue culture plate containing 2 x 10^5/mL "665" E_μ-Myc cells per well, or 665 cells were treated with 0.5 ng/mL recombinant mouse CCL19 for 24 hr. Non-viable cells were identified via trypan blue exclusion and excluded from the cell count. No loss of viability was noted for any of the treatment paradigms. To create *Cxcr4*$^{-/-}$ 665 cells, single guide RNA sequences were retrieved from https://chopchop.cbu.uib.no/ (Labun et al., 2016; Montague et al., 2014). Guides were cloned into the lentiCRISPR v2 backbone (Sanjana et al., 2014) by means of golden gate assembly (Engler et al., 2008). HEK293T cells were transfected with guides and empty vector control together with lentiviral packaging vectors and lipofectamine. Viral supernatant was harvested twice after 18h and 36h and used to spin transduct the 665 E_μ-Myc lymphoma cell line twice (500 g; 60 min). After 24h, puromycin selection (3 μg/mL, 10 days) was commenced. Controls died within 3 days. CXCR4 surface expression was measured via FACS and compared to empty vector control. Guides 1 and 2 were chosen for further experiments. ACH6 (Biogen Idec) was used at 5 μg/mL. Recombinant mouse TNFα (Thermofisher) was used at 10 – 20 ng/mL. For binding experiments, sEnd.1 cells were treated for 16 hr with 5 μg/mL ACH6 on coverslips and then incubated for 1 hr. with 1 × 10^5 E_μ-Myc lymphoma cells. Unbound cells were washed away with PBS, and cultures were then fixed in 4% formalin. The number of B220-positive cells in three non-overlapping images per well was averaged and expressed as % Ctrl. For transmigration experiments, 1 × 10^6 "WT" or *Ccr7*$^{-/-}$ 665 cells were cultured in 200 μL complete RPMI in the upper well of a 5 μm transwell insert (Costar # 3421) with 600 μL complete RPMI in the lower chamber. "Ctrl" cells contained no chemokines in the upper or lower chamber. "CXCL12" cells contained 200 ng/mL CXCL12 in the lower chamber. "CXCL12 + CCL19" cells contained 400 ng/mL CCL19 in the upper chamber (pre-treated for 10 min. prior to experiment start) and 200 ng/mL CXCL12 in the lower chamber. 10 μL of media in the lower chamber was taken at 0, 2, 6, and 24 hr after the start of the experiment, and the number of 665 cells transmigrating into the lower chamber was quantified with a Neubauer chamber and expressed as a percentage of total cells in the experiment. 4 wells per treatment group were measured at each time point. For AMD3100 control experiments, cells were pre-treated with 10 μg/mL AMD3100 (Sigma) for 10 min, prior to addition of CXCL12. All cell culture reagents were purchased from Thermofisher unless otherwise specified.

FACS

For standard FACS, 1 x 10^6 665 cells were washed in 1 mL FACS buffer (0.5% BSA in 1x PBS) and re-suspended in 50 μL FACS buffer containing 20 μg/mL FITC-CD49d, FITC-Rat IgG2b isotype control, AlexaFluor 488-CCR7, AlexaFluor 488-Rat IgG2a Isotype control, FITC-CD11a, FITC-CXCR5, CXCR4, or Rat IgG2b Isotype control. Cells were stained for 30 min. on ice in the dark. Cells were then washed in FACS buffer and re-suspended in 400 μL 1 μg/mL DAPI staining solution. Labeled cells were analyzed using a Beckman Coulter CyAn ADP. For whole-brain FACS analysis, brains were collected and incubated on ice in RPMI. Brains were minced and digested at 37°C for 30 min. with 1:100 collagenase D and 1:200 DNAase diluted in RPMI. After digestion, brains were passed through a 100 μm cell strainer, washed 2x with RPMI, and re-suspended in 4 mL of FACS buffer and subjected to density gradient centrifugation using 4 mL Pancoll and 2 mL Percoll and at 2200 rpm for 30 min. at 4°C; acceleration 7; deceleration 1. The leukocyte ring was collected in a new 15 mL Falcon tube, washed with FACS buffer, and collected by centrifugation. The lymphocyte pellet was resuspended in 300 μL RPMI, and incubated with PE/Dazzle-conjugated B220, BV421-conjugated CD11c and CD11b, PE-CD3, AlexaFluor 700-conjugated CD45, counting beads, and Zombie live/dead stain (Biolegend) and incubated for 20 min. at 4°C. Stained cells were centrifuged, re-suspended in 100 μL FACS buffer, and measured on a BD Fortessa FACS machine. Gated live cell populations were $CD45^+$, $B220^+$, $CD3^-$, $CD11b^-$, and $CD11c^-$. Absolute numbers were obtained by normalizing to counting beads. Representative gates for each genotype are shown in Figure S2K.

Immunocytochemistry

Adherent cells on coverslips were fixed for at least 20 min. in 4% formalin. Cells were rinsed with 1x PBS and then permeabilized in 0.3% Triton-X 100 for 5 min. at room temperature. Cells were then rinsed with 1x PBS and incubated for 30 min. at room temperature in 5 mM DTT, 0.1% SDS in 1x PBS. Cells were rinsed with 1x PBS and blocked for 40 min. in 1% FBS. Cells were then washed 2x in 1% BSA in 0.25% Triton-X-100 in 1x PBS. Cells were then incubated in 2 μg/mL anti-CD31 and 0.17 μg/mL anti-B220 or 20 μg/mL CCL19 and 1:500 early endosomal marker EEA1 or 1:1000 mouse monoclonal GFAP diluted in 1% BSA in 0.25% Triton-X 100 in 1xPBS overnight at 4°C. Cells were then washed 1x with 1x PBS and 2x with 1% BSA in 0.25% Triton-X 100 in 1xPBS. Cells were then incubated for 2 hr with 2 μg/mL AlexaFluor 488-conjugated goat anti-rabbit and AlexaFluor 594-conjugated goat anti-rat or AlexaFluor 488-conjugated donkey anti-goat followed by (to avoid cross-reactivity) AlexaFluor 594-conjugated goat anti-rabbit or goat anti-mouse diluted in 1% BSA in 0.25% Triton-X 100 in 1xPBS containing 1:10,000 DAPI. Cells were washed 2x in 1x PBS and mounted with Dako fluorescent mounting media. For non-adherent cells, 1 × 10^6 cells were fixed for 15 min. in 4% formalin, washed

with 1x PBS, stained for 30 min. with 1 μg/mL FITC-conjugated CD11a or CD49d, washed with 1x PBS, re-suspended in 2 drops of Dako fluorescent mounting media, and transferred to a glass slide and coverslipped. Cells were imaged once they had settled onto the microscope slide. Epifluorescent images were taken with an Olympus BX53 fluorescent microscope, and confocal images were taken with a Leica SP5.

Real Time PCR

Tissues were flash frozen in liquid nitrogen and stored at -80°C. Frozen tissues were later homogenized in Qiazol (Qiagen) or PeqGOLD Trifast (10% w/v) using a GentleMACS Dissociator (Miltenyi Biotech) and subjected to chloroform extraction, whereas cells were lysed with 1% β-mercaptoethanol in RLT buffer (Qiagen). Total mRNA was isolated using an RNeasy Mini kit (cells) or an RNeasy Lipid Mini Kit (tissues), according to the manufacturer's instructions (Qiagen). 1 μg mRNA from each sample was used for first-strand cDNA synthesis using random hexamers from a Qiagen Quantitect kit and diluted 1:100. 1.5 μL cDNA, 500 nM primers, and 1x Faststart SYBR Green reaction mixture (Applied Biosystems) in 12.5 μL reaction volumes were used for Real Time PCR amplification of target sequences from tissues normalized to GAPDH using an ABI 7900HT (Applied Biosystems). (See Tables S2 and S3 for list of primer sequences.) Reactions from each tissue were performed in triplicate and averaged. Amplification data was analyzed using the relative quantification method (RQ) where test samples are expressed relative to the average of the control values, and the average RQ of the control values = 1. Average values depicted in the graphs represent the mean value of single tissues from each individual mouse or well (cells) from each treatment group.

LTα ELISA

A 96-well NUNC Maxisorp ELISA plate was incubated overnight at 4°C with 5 μg/mL per well of anti-LTα (clone s5H3.2.2) in ELISA coating buffer (0.1M $NaHCO_3$, 0.1 M Na_2CO_3, pH = 9.6), washed (0.05% Tween-20 in 1x PBS), blocked for 1 hr at room temperature with 5% BSA in 1x PBS, and washed five additional times. LTα recombinant protein (10 – 0.156 ng/mL; 749-TB-025; R&D Systems) or 25 μg total protein homogenate (diluted in blocking buffer) of each sample was added to the plate in duplicate and then incubated at 4°C overnight. Plates were washed five times and incubated with 50 ng/mL anti-LTα (R&D Systems) diluted in blocking buffer for 2 hr at room temperature. Plates were washed five times and then incubated for 30 min. at room temperature with 1:500 Avidin-HRP (18-4100-51; eBiosciences) in blocking buffer. Plate was washed five times and then incubated with 50 μL/well TMB solution (00-4201-56; eBiosciences) for 30 min. The colorimetric reaction was stopped with 20% H_2SO_4, and the absorbance values were determined with a Tecan plate reader at 450 nm. Values were expressed as ng LTα protein detected in each sample (as determined from the standard curve) per mg of total protein in each sample (as determined by the BCA method).

CCL19 ELISA

Murine CCL19 ELISA was purchased from R&D Systems and performed according to the manufacturer's instructions. Primary glial cells treated for 48 hr with 10 – 20 ng/mL murine TNFα, 5 μg/mL ACH6, or 20 ng/mL TNFα + 5 μg/mL ACH6 in a 24-well plate were lysed in 200 μL 1% Triton-X-100 in 1x PBS supplemented with protease inhibitors (Complete Mini; Roche). Cell lysates were divided and added to the ELISA plate in duplicate. 10% (w/v) brain homogenates were created with 1% Triton-X-100 in 1x PBS supplemented with protease inhibitors from flash frozen brain tissue lysed with a TissueLyser (Miltenyi), diluted 1:4 with sample diluent provided in the kit. Samples were added to the ELISA plate in duplicate, averaged, and expressed as pg of total CCL19 protein per mg of total protein in the lysate (as determined by BCA; Pierce). Human CCL19 ELISA was purchased from R&D Systems and performed according the manufacturer's instructions. Human CSF samples were diluted 1:2 in sample diluent (provided in kit), added to the ELISA plate in duplicate, and incubated overnight at 4°C. Values are expressed as pg/mL of CCL19 in undiluted CSF.

Immunohistochemistry, Quantifications, and 3D Reconstructions

Tissues were drop-fixed in 4% neutral buffered formalin for a minimum of 24 hr and then paraffin-embedded. 2 μm sections were cut from paraffin blocks with a microtome, mounted on glass coverslips (Thermofisher), and stained using a Leica BOND-MAX automated staining machine (See Table S4 for list of primary antibodies and dilutions). Stains were developed with 3,3'-diaminobenzidine (DAB) and/or Fast Red (Sigma), counter-stained with hematoxylin and eosin (H&E), cleared with xylol, mounted, and imaged with an Olympus BX53 light microscope. For quantification of CNS lymphomas or individual lymphoma cells, brains were dissected sagittally between the two hemispheres, and cuts closest to the midline were immunostained with B220 or B220 + CD31. Total numbers of $B220^+$ cell clusters were counted within each brain section, as well as the total number of $B220^+$ cells within each cluster. Meningeal and intravascular lesions were excluded from this analysis. For short-term experiments, total numbers of $B220^+$ cells per brain section were counted. For B220 + CD31 quantifications, the total ratio of $CD31^-$ (i.e. parenchymal) $B220^+$ cells versus $CD31^+$ (i.e. clearly overlapping or within an AP-stained vascular structure) was quantified per brain section. $B220^+$ cells in the meninges were excluded from this analysis. A minimum of n = 5 different mice per experimental group was analyzed for every experiment. For non-tumor IHC quantifications, % positive area was calculated in ImageJ using the "Measure" function. For 3D images shown in Figure 1C, 30 μm paraffin sections were stained 1:500 for 48 hr at 4°C with GFAP antibody (Abcam ab4674) followed by overnight incubation with AlexaFluor 647 secondary antibody. Images were captured with an Olympus Fluoview 1000 confocal microscope, and image analysis was performed in Imaris. For 3D images in Figure 3B, 25 – 30 serial 2 μm paraffin sections from brains of terminal GFAP-LTαβ or IKK2CA mice injected with E_μ-Tcl1 cells were stained for B220 and counter-stained with H&E. The same ROI from each brain section was imaged and aligned using the CwR ImageJ plugin developed by Dr. Ching-Wei Wang: http://www-o.ntust.edu.tw/~cweiwang/

ImageRegistration/ (Wang et al., 2014). Aligned images were cropped and stacked using ImageJ, and 3D images were created using the Volume Viewer plugin for ImageJ (Schneider et al., 2012).

Immunofluorescence and Quantifications

Tissues were flash frozen in liquid nitrogen in O.C.T. medium (Tissue-Tek) and stored at -80°C. Tissues were later cut into 10 μM frozen sections with a cryostat (Leica), mounted on glass coverslips, and stored at -20°C. Prior to staining, sections on coverslips were dried for several hours at room temp and then fixed in 4% formalin for 2 min, 50% acetone for 2 min, 100% acetone for 2 min, and 50% acetone for 2 min. For nuclear stains (i.e. Tcl1), acetone steps were omitted, and formalin incubation time was increased to 5 min. Sections were then washed in 1x PBS, then 1x PBS + 0.1% Tween 20, and blocked for 1 hr. in SuperBlock (Pierce). For stains with mouse monoclonal antibodies, 5% mouse serum was added to the blocking step. Sections were then incubated overnight at 4°C in primary antibody (See Table S5 for a list of primary antibodies) diluted in 1:10 SuperBlock. Sections were then washed in 1x PBS, followed by 1x PBST, then incubated with 2 μg/mL Alexa Fluor-conjugated secondary antibody (Thermofisher) diluted in 1:10 SuperBlock containing 1:10,000 DAPI for 1 hr. at room temperature. Control stains with one or the other primary antibody omitted were performed to test for cross-reactivity. Sections were then washed in 1x PBS followed by 1x PBST, mounted with fluorescent mounting medium (Dako), coverslipped, and imaged with an Olympus BX53 fluorescent microscope. Spearman's rank correlation coefficient to estimate the degree of co-localization in co-immunofluorescent images was determined using the "Coloc2" program in Fiji (Schindelin et al., 2012). Human cryo tissue was stained 1:50 witih anti-human CCL19 (R&D Systems), 1:250 CD20 (Abcam), 1:50 CCR7 (Sigma) overnight, or 1:1000 GFAP (Sigma # G6171) for 1 hr.

Western Blots and Cytokine Arrays

10% (w/v) protein homogenates were made from flash frozen brain tissue in 1% Triton-X 100 in 1x PBS supplemented with a protease inhibitor cocktail (Roche Complete Mini) using a gentleMACS tissue dissociator (Miltenyi). Total protein determination was made using the BCA method (Pierce). For cytokine arrays, 200 μg NTg or GFAP-LTαβ homogenates were incubated with Mouse XL (R&D Systems) cytokine array membranes according to the manufacturer's instructions. For Western blots, 10 μg protein homogenates were diluted in 1x Laemmli buffer (BioRad), heated to 95°C for 5 min, centrifuged, and loaded onto 4-12% Bis-Tris NuPage gels (Thermofisher), and electrophoresed at 50-100V. Proteins were transferred to 0.45 μm nitrocellulose (GE Healthcare) at 100V for 1 hr in transfer buffer (25 mM Tris base, 0.192 M Glycine) + 20% methanol using a BioRad transfer apparatus. Transferred blots were rinsed in 1X Tris-buffered saline (50 mM Tris-HCl, pH = 7.5; 150 mM NaCl) with 0.1% Tween 20 (TBST), blocked for 1 hr. in 5% (w/v) dried milk powder in 1X TBST, incubated for 1 hr. with GFAP (clone G-A-5) diluted 1:2000 and GAPDH antibodies diluted 1:1000 or N-Cadherin diluted 1:1000 in 5% milk in 1X TBST. Blots were washed in 1X TBST and then incubated with horse radish peroxidase-conjugated goat anti-rabbit and anti-mouse secondary antibodies (Cell Signaling #7076 and #7074) diluted 1:10,000 in 5% milk in 1X TBST. Blots were washed with 1X TBST and developed with BioRad Clarity enhanced chemiluminescent reagent. Chemiluminescent signals were developed with a BioRad ChemiDoc XRS+, and densitometric analysis was performed using Image Lab (BioRad).

Analyzing Blood Brain Barrier Integrity

For analysis of blood-brain barrier leakage, cryosections from WT and GFAP-LTαβ mice were co-stained with 1:800 anti-albumin and 1:1000 GFAP primary antibodies followed by 1:800 AlexaFluor 488 and AlexaFluor 555. For Evans blue experiments, mice were injected i.p. with 200 μL 2% (w/v) Evans blue dye dissolved in sterile 1x PBS. 6 hr later, mice were transcardially perfused with 1x PBS, and dye penetration of the brain was analyzed visually. Positive control mice received whole-body irradiation. For electron microscopy, tissue was fixed in 3% glutaraldehyde in Sörensen phosphate buffer and embedded in araldite, and subsequently cut into ultra-thin sections. Ultrastructural analysis was performed using CM100 transmission electron microscope (Philips).

In Vivo Bioluminescence

E_μ-Myc cells were transduced with a lentiviral vector co-expressing dsRed and firefly luciferase. Cells with the highest dsRed expression were selected using a Sony SH800 cell sorter. 1×10^7 luciferase-expressing E_μ-Myc cells were injected i.v. into GFAP-LTαβ or NTg mice. 30 min. post-injection, mice were injected i.p. with 160 mg/kg of luciferin, anesthetized with isoflurane, and total bioluminescence in the brain (in photons / sec / cm^2 / sr) was measured 10 min. post-injection with an IVIS Lumina III *in vivo* imaging system (PerkinElmer).

In Vivo Two-Photon Microscopy

Two-month old C57BL/6 WT or GFAP-LTαβ mice were surgically fitted with a 6 mm Ø cortical glass window as previously described (von Baumgarten et al., 2011). Approximately 4 weeks post-surgery E_μ-Myc cells were labeled with 10 μM CellTracker Red CMTPX (Thermofisher) for 30 min. Mice were injected i.v. with 1 mg FITC-dextran and 1.5×10^7 CMTPX-labeled E_μ-Myc cells. Two hours post-injection, mice were anesthetized with isoflurane, and brains were imaged using a Multiphoton TrimScope I system (LaVision BioTec; Bielfeld, Germany) coupled to an upright Olympus microscope equipped with a MaiTai Laser (690 – 1040 nm; Spectra Physics; Santa Clara, CA, USA), and 20x water immersion objective (numerical aperture 0.95; Olympus XLUMPlandFl) with double distilled water used as an immersion medium. The MaiTai laser was tuned to 800 nm to visualize FITC-dextran and CMTPX simultaneously. Brain images were taken every 3 μm up to a depth of 500 μm at six randomly selected regions of interest. The same ROIs were re-imaged at 24 and 48, and (in some cases) 72 hr post-lymphoma cell injection. *Ccr7*$^{-/-}$ E_μ-Myc cells were created by targeting three

individual sequences within exon 2 of murine CCR7 (NM_007719) for CRISPR/Cas9-mediated deletion. Pure populations of *Ccr7*$^{-/-}$ E_μ-Myc cells were isolated via negative selection with a Sony SH800 cell sorter and AlexaFluor 488-conjugated CCR7 antibody. A total of 309 E_μ-Myc cells in four WT brains, 525 E_μ-Myc cells three GFAP-LT$\alpha\beta$ brains, and 774 *Ccr7*$^{-/-}$ E_μ-Myc cells in three GFAP-LT$\alpha\beta$ brains were analyzed. Images were analyzed and processed using ImageJ and Imaris. For videos, raw images were imported as a .Tiff series in Fiji 1.0. Single channels were split, and the background was adjusted using the subtract background function (rolling ball radius at 50.0 pixel) and gaussian filter (sigma radius at 2.00) and finally exported as 16-bit .tiff images. Each channel was imported into Imaris (bitplane) for the 3D rendering, and videos were recorded at 10 frames per second. Video montages and annotations were inserted by iMovie (Apple).

QUANTIFICATION AND STATISTICAL ANALYSIS

Statistical analyses were performed using GraphPad Prism. Calculation of significant differences between groups for disease incidence was performed using a Chi square test. All other experiments were analyzed using a Student's t-test. Error bars in graphs indicate the standard error of the mean (± S.E.M.) Statistical significance was indicated by: *$p < 0.05$, **$p < 0.01$, ***$p < 0.001$ in the figures. Sample sizes are indicated in the figure legends. For *in vivo* experiments, n indicates individual mice. For cell culture experiments, n indicates individual wells of cells in a cell culture plate which were plated, treated, lysed, and analyzed separately.

DATA AND CODE AVAILABILITY

Mass spectrometry-based proteomic analyses have been deposited on the Proteomics Xchange Consortium, identifier # PXD014099.